이학박사 학위논문

Complex inner core of the Earth constrained by differential travel times and differential ray parameters

주시와 파선 변수 차를 이용한 지구 내핵 구조 연구

2017년 2월

서울대학교 대학원

지구환경과학부 지진학전공

이 태 규

Abstract

Studies of velocity structure in the Earth's inner core and its volumetric variations illuminate our understanding of inner core dynamics and composition. Here I use an extensive number of seismograms recorded by the Hi-net array to construct complete empirical curves of PKPbc-PKPdf differential traveltimes. The nature of these curves implies that significant variations in traveltimes are accumulated during the passage of PKPdf waves through the uppermost inner core, and rules out outer core structure effects. Uniform cylindrical anisotropy of a plausible strength in the uppermost inner core can also be ruled out as a cause of the observed travel-time variations because the range of sampled ray angles is too narrow. The configuration and strength of inhomogeneities from a recent tomographic model of the lowermost mantle cannot account for the observed travel-time variations. Therefore, I infer that either variations of P-wave isotropic velocity on the scale of about hundred km and less are present in the uppermost inner core or the material may be organized in distinctive anisotropic domains, and both of these features may be superimposed on long-wavelength hemispherical structure. If the former holds true, the absolute magnitude of required P-wave velocity perturbations from referent values is

0.60±0.10% in the quasi-eastern and 1.55±0.15% in the quasi-western hemisphere (0.85±0.05% and 1.10±0.10%, respectively, with the lowermost mantle correction). The existence of these variations is a plausible physical outcome given that vigorous compositional convection in the outer core and variations in heat-exchange across the inner core boundary may control the process of solidification. Although I show the existence of heterogeneity on regional scale, the precise location and size of heterogeneities could not be constrained using exclusively the perturbed differential travel times. To overcome this limitation, here I utilize the PKPbc-PKPdf differential ray parameters in addition to the corresponding differential travel times to study the Vp structure of the uppermost inner core. I find that the differential ray parameters measured by phase-weighted stacking of waveforms recorded by the Hi-net array also display regional variations in both quasi-hemispheres. This observation supports previous results and provides additional constraint on complex Vp structure. I examine a number of 2-D models with different nature of heterogeneities including the inner core boundary topography and a mushy zone to predict the observed regional variation of the differential travel times and differential ray parameters. Our estimates of the heterogeneity spectrum represent invaluable new constraints on inner core structure.

Keywords: Earth’s inner core, PKPdf, PKPbc, differential traveltime, differential ray parameter, P-wave velocity variation; isotropic heterogeneity, phase-weighted stack

Student Number: 2010-30110

Contents

List of Tables

List of Figures

Chapter 1

Introduction

Since the discovery of the inner core (IC) [*Lehmann*, 1936], various spherically symmetric (1D) P-wave velocity models of the IC have been proposed [e.g., *Jeffreys*, 1939; *Müller*, 1973; *Qamar*, 1973; *Anderson and Hart*, 1976; *Dziewonski and Anderson*, 1981; *Kennett and Engdahl*, 1991; *Kennett et al*., 1995]. However, it was suggested by *Poupinet et al*. [1983] that the IC might have a prolate shape to explain differences in traveltimes of PKIKP waves traversing the IC and then A concept of a uniform cylindrical IC anisotropy stems from this observation and was used to explain travel-time anomaly observed in PKP_{DF} waves [*Morelli et al*., 1986] and anomalous splitting of normal modes sensitive to IC structure [*Woodhouse et al*., 1986]. Since then various seismological studies have been conducted in conjunction with IC anisotropy on a global scale [e.g. *Shearer and Toy*, 1991; *Tromp*, 1993; *Romanowicz et al.*, 1996; *Song and Helmberger*, 1998], its quasi-hemisphericity [e.g. *Tanaka and Hamaguchi*, 1997; *Creager*, 1999; *Garcia and Souriau*, 2000; *Niu and Wen*, 2002; *Irving and Deuss*, 2011], its radial variation [e.g. *Ishii and*

Dziewonski, 2002; *Calvet et al*., 2006; *Cormier and Stroujkova*, 2005] and its regional variation [e.g. *Isse and Nakanishi*, 2002; *Helffrich et al*., 2002; *Tkalčić*, 2010].

Meanwhile, observational evidence from a number of studies supports a laterally heterogeneous IC. Various scales of IC heterogeneities have been reported in a better sampled, top part of the IC: quasi-hemispheric [e.g. *Tanaka and Hamaguchi*, 1997; *Niu and Wen*, 2001; *Yu et al*., 2005], regional [e.g. *Kaneshima*, 1996; *Stroujkova and Cormier*, 2004; *Krasnoshchekov et al*., 2005], and fine-scale structures [e.g. *Creager*, 1997; *Cormier and Li*, 2002; *Leyton and Koper*, 2007a; *Peng et al*., 2008]. The hypothesis that the top of the IC is a mushy zone seems to be well established [e.g. *Cao and Romanowicz*, 2004], with the estimated grain-size on the order of 1-2 km [e.g., *Vidale and Earle*, 2000] and the scale-length of volumetric heterogeneities in the uppermost inner core (UIC) on the order of 1-10 km [*Leyton and Koper*, 2007a]. Even smaller grain size of several hundred meters was suggested by *Calvet and Margerin* [2008] and *Cormier and Li* [2002] estimated several hundred meters near the top of the IC, increasing with depth up to 10's of km.

With the increase of data and the development of observational technology, the inner core of the earth is getting more complicated, but the problem is that the results are not in good agreement. This naturally led to the speculation that the structure of the inner core would be very complicated regionally and locally, but we still have insufficient understanding about this argument. In order to overcome this problem, we use high dense arrays and array-based techniques here. This work is entirely based on a new dataset collected by a dense array of seismic stations with a goal of mapping structure in the UIC. It gives a glimpse of what can be achieved in deep Earth seismology with a large number of newly collected data and some of the well-established techniques. It leads to a conclusion that the UIC is regionally heterogeneous.

In chapter 2, regionally heterogeneous uppermost inner core observed with Hi-net array, we collect PKP travel-times corresponding to ray-paths that span epicentral distance range from 147° to 155° such that both PKIKP (PKP_{DF}) and PKP_{BC} phases are clearly recorded on the same seismogram and then analyze BC-DF residuals with respect to spherically-symmetric reference models of the Earth. We verify by forward synthetic tests that different velocity profiles in the lowermost outer core, heterogeneities in the outer core and the lowermost mantle, which could all hypothetically have significant impact on BC-DF. Our

analysis results in 47 individual 1D structural models (velocity profiles as a function of depth) that represent distinct volumes of the UIC. When these profiles are considered together, they are in agreement with a hemispherical dichotomy in the UIC, but also argue for regional variations in isotropic velocity with around 1% amplitude in each quasi-hemisphere. We then discuss the observed velocity profiles and their lateral variation in the context of previous seismological and geodynamical work and conclude with ideas for future work directions.

In chapter 3, Complex inner core of the Earth constrained by differential ray parameters, we discuss about the limitation of uncertainties of differential traveltimes and examine how these uncertainties and the non-uniqueness of the differential traveltimes have a significant influence on the velocity structure determination. Then we perform Phase-Weighted Stack (PWS) for same waveforms as Yee et al [2014] to obtain both, the differential traveltimes and the differential ray parameters and try to confirm that the differential traveltimes obtained from the PWS method is same with previous ones from the cross correlation method. The variations of the differential ray parameters demonstrate that the importance of considering the ray parameters with traveltimes and the existence of regional heterogeneities in the inner core. We

investigate other possibilities and discuss about further studies to match these high-dimensional features.

Chapter 2

Regionally heterogeneous uppermost inner core observed with Hi-net array

1. Introduction

Since the discovery of the inner core (IC) [*Lehmann*, 1936], various spherically symmetric (1D) P-wave velocity models of the IC have been proposed [e.g., *Jeffreys*, 1939; *Müller*, 1973; *Qamar*, 1973; *Anderson and Hart*, 1976; *Dziewonski and Anderson*, 1981; *Kennett and Engdahl*, 1991; *Kennett et al*., 1995]. Although these models present an accurate description of a wide range of geophysical data, observational evidence from a number of studies supports a laterally heterogeneous IC. Various scales of IC heterogeneities have been reported in a better sampled, top part of the IC: quasi-hemispheric [e.g. *Tanaka and Hamaguchi*, 1997; *Niu and Wen*, 2001; *Yu et al*., 2005], regional [e.g. *Kaneshima*, 1996; *Stroujkova and Cormier*, 2004; *Krasnoshchekov et al*., 2005], and fine-scale structures [e.g. *Creager*, 1997; *Cormier and Li*, 2002; *Leyton and Koper*, 2007a; *Peng et al*., 2008]. The hypothesis that the top of the IC is a

mushy zone seems to be well established [e.g. *Cao and Romanowicz*, 2004], with the estimated grain-size on the order of 1-2 km [e.g., *Vidale and Earle*, 2000] and the scale-length of volumetric heterogeneities in the uppermost inner core (UIC) on the order of 1-10 km [*Leyton and Koper*, 2007a]. Even smaller grain size of several hundred meters was suggested by *Calvet and Margerin* [2008] and *Cormier and Li* [2002] estimated several hundred meters near the top of the IC, increasing with depth up to 10's of km. Both of these estimates come from interpreting inner core Q as a scattering Q that broadens the PKP_{DF} pulse by transferring scattered high frequency into the later coda. *Deguen et al*. [2007] suggest that due to uncertainties in conjunction with iron conditions at high temperature/pressure, it is difficult to estimate the thickness of a mushy zone.

Apart from the process of solidification, the IC is experiencing a post-solidification deformation due to an internal stress field [e.g. *Jeanloz and Wenk*, 1988; *Yoshida et al*., 1996] and it is not entirely clear which one of these two processes has a dominant impact on crystal growth and IC texture. *Cormier* [2007] and *Cormier et al*. [2011] argue that an outward-stretched (radial) or inner core boundary (ICB) parallel-stretched (tangential) heterogeneity in the UIC can reconcile some observations of IC hemisphericity in seismic

attenuation and scattering from PKiKP wave coda [*Leyton and Koper*, 2007b]. Their results are in line with the hypothesis that the quasi-eastern hemisphere (QEH) is freezing faster than the quasi-western hemisphere (QWH) [*Aubert et al*., 2008]. Although in odds with this scenario, a hypothesis of *Monnereau et al.* [2010] and *Alboussière et al.* [2010] that the QEH is melting faster than the QWH is still consistent with the observed attenuation dichotomy between the two hemispheres of the IC [e.g. *Cao and Romanowicz*, 2004]. Crystal size in the QEH might be larger than typical wavelengths of body waves sensitive to IC structure and this can explain observed lack of strong back-scattering [*Leyton and Koper*, 2007b], while the melting component can explain higher attenuation. An alternative model would be an isotropic distribution of scale lengths in places where PKiKP coda has been observed in the mid-Pacific, and possibly a larger crystal (or organized patch of crystals) in regions where no strong PKiKP coda is observed [*Cormier et al*., 2011].

That the above-described dichotomy in seismic velocity (and seismic attenuation) exists between the two hemispheres of the IC is largely based on the travel-times and amplitudes of body waves sampling the IC in the equatorial region. In a recent study, however, *Ohtaki et al*. [2012] demonstrate that the IC does not have a simple hemispherical variation. Their analysis, while not global

but based on unique ray-path sampling of the IC under Antarctica, supports a single eyeball-shaped anomaly concentrated onto a small region beneath eastern Asia.

Much less constrained by seismic data than seismic velocity and attenuation, is seismic anisotropy. *Poupinet et al.* [1983] observed that PKP_{DF} waves travel faster along the quasi-polar than the quasi-equatorial paths through the IC. A concept of a uniform cylindrical IC anisotropy stems from this observation and was used to explain travel-time anomaly observed in PKP_{DF} waves [*Morelli et al*., 1986] and anomalous splitting of normal modes sensitive to IC structure [*Woodhouse et al*., 1986]. Since then various seismological studies have been conducted in conjunction with IC anisotropy on a global scale [e.g. *Shearer and Toy*, 1991; *Tromp*, 1993; *Romanowicz et al.*, 1996; *Song and Helmberger*, 1998], its quasi-hemisphericity [e.g. *Tanaka and Hamaguchi*, 1997; *Creager*, 1999; *Garcia and Souriau*, 2000; *Niu and Wen*, 2002; *Irving and Deuss*, 2011], its radial variation [e.g. *Ishii and Dziewonski*, 2002; *Calvet et al*., 2006; *Cormier and Stroujkova*, 2005] and its regional variation [e.g. *Isse and Nakanishi*, 2002; *Helffrich et al*., 2002; *Tkalčić*, 2010]. For more details, see recent review papers [*Souriau*, 2007; *Tkalčić and Kennett*, 2008; *Cormier et al*., 2011; *Deguen*, 2012].

A recent progress in normal mode techniques considering mode coupling [e.g. *Deuss et al.*, 2010], is in agreement with findings from body waves that point to complex structure in the IC superimposed on simpler long-wavelength average structure. Normal modes, however, are sensitive to relatively long spatial scales, comparable with the IC radius and hence constrain average structure, much less insights in fine structure that might characterize the UIC. Therefore, body wave techniques continue to be essential tool in our quest to better understand geodynamical processes near the boundary between the solid and the liquid part of the core.

In contrast to normal modes, seismological techniques associated with body wave travel-time data have remained relatively unchanged over the last several decades. For example, an advantage of measuring differential travel-times over absolute travel-times has been demonstrated in numerous studies and this remains one of the most exploited techniques since the pioneering work [e.g. *Cormier and Choy*, 1986]. The computational power is still insufficient to synthesize the seismic wavefield at 1 Hz and above for inner core-related seismic phases including the full range of 3-D influences in the mantle and inner core.

Thus, while it appears that seismological studies still have a long way to go before the reconciliation of various results can be made, the characterization and mapping of heterogeneity in the IC remains an important topic. Fortunately, what has changed dramatically in the last decade is the number of seismic recorders around the world, and therefore the capacity and potential to measure more travel-times of core-sensitive body waves. Moreover, high dense arrays and array-based techniques probably represent future of seismic studies of the deep Earth's interior. For a more detailed account on array studies, see a review by *Rost and Thomas* [2002]. This work is entirely based on a new dataset collected by a dense array of seismic stations with a goal of mapping structure in the UIC. It gives a glimpse of what can be achieved in deep Earth seismology with a large number of newly collected data and some of the well-established techniques. It leads to a conclusion that the UIC is regionally heterogeneous.

Our array of choice with unprecedented density of elements, all installed in boreholes, is the Hi-net array of short period instruments located in Japan. The array has significantly higher signal to noise ratio in comparison with the stations at the surface. We exploit the position of the Hi-net array and the corresponding regions of the UIC sampled by the ray-paths of PKP waves

recorded with the Hi-net array elements (Section 2). We collect PKP travel-times corresponding to ray-paths that span epicentral distance range from 147° to 155° such that both PKIKP (PKP_{DF}) and PKP_{BC} phases are clearly recorded on the same seismogram (Figure 2.1). The finally selected dataset consists of 47 individual events (from initial 242 ones), whose ray-paths provide a dense coverage of the UIC. This allows us to construct complete empirical travel-time curves of PKP_{BC}-PKP_{DF} differential travel-times (hereafter called BC-DF). We then analyze BC-DF residuals with respect to spherically-symmetric reference models of the Earth (Section 3).

Firstly, we exclude a possibility that uniform cylindrical anisotropy in the UIC has a significant effect on the observed BC-DF travel-times. This follows from the fact that the span of the angles between the ray-paths of PKP_{DF} in our dataset and the rotation axis of the Earth is too narrow for anisotropy to have any noticeable effect (Section 4.1.). Our analysis results in 47 individual 1D structural models (velocity profiles as a function of depth) that represent distinct volumes of the UIC. When these profiles are considered together, they are in agreement with a hemispherical dichotomy in the UIC (Section 4.2.), but also argue for regional variations in isotropic velocity with around 1% amplitude in each quasi-hemisphere (Section 4.3.). We verify by forward

synthetic tests that different velocity profiles in the lowermost outer core (Section 4.4.), heterogeneities in the outer core and the lowermost mantle (Section 4.5.), which could all hypothetically have significant impact on BC-DF, do not explain the observed variations. We then discuss the observed velocity profiles and their lateral variation in the context of previous seismological and geodynamical work (Section 5) and conclude with ideas for future work directions (Section 6).

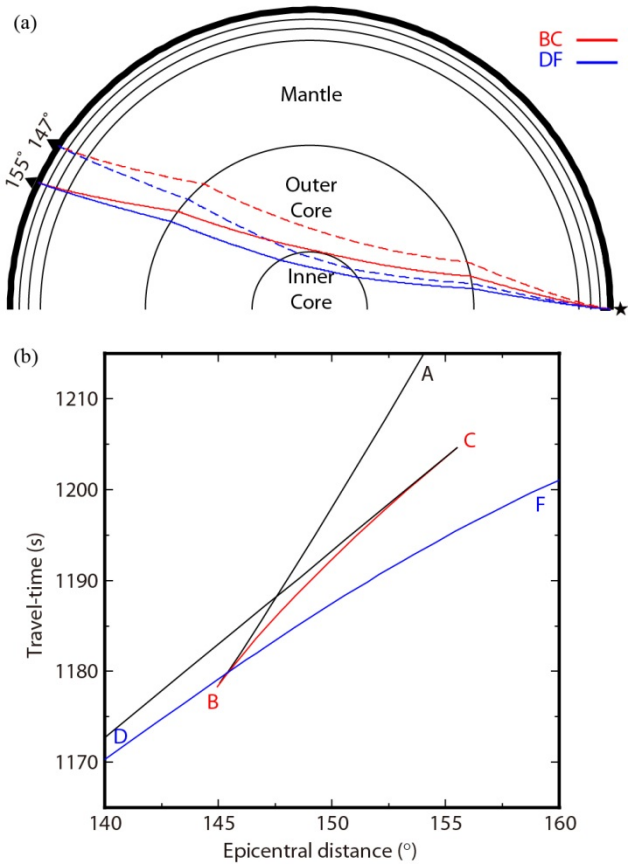

Figure 2.1. (a) Ray-paths of PKP_{DF} (blue lines) and PKP_{BC} (red lines) at epicentral distance of 147° (dashed lines) and 155° (solid lines). Star and triangle symbols indicate epicenter and station locations. (b) Travel-time curves of PKP waves around a triplication predicted from ak135 model [*Kennett et al*., 1995].

2. Data

The data considered in this study are collected from vertical component seismograms recorded at the high sensitivity seismograph network (Hi-net) consisting of about 800 stations operated by the National Research Institute for Earth Science and Disaster Prevention (NIED) in Japan. The high sensitivity seismometers are installed at depths of 100 m or deeper inside the boreholes to observe stable seismic waveforms by reducing surface ground noise. The Hi-net array elements cover the entire area of Japan with an average spacing of about 20 km [*Okada et al*., 2004]. The configuration of Hi-net array and the location of large teleseismic earthquakes beneath southern Indian and northeastern Pacific Oceans deliver ray-paths with near-equatorial sampling of the IC that span the epicentral distance range between 147° and 155° and sample both QEH and QWH of the IC. The fact that the Hi-net array is superabundant and favorably positioned to allow the recording of the core-sensitive wave-field presents an unprecedented opportunity to study the Earth's core "with a high-resolution lens". Several studies focusing on anisotropy, attenuation and other seismic structures of the IC using Hi-net data demonstrated the reliability and merit of various observations in the investigation of the deep Earth structure [e.g. *Kawakatsu*, 2006; *Kazama* et al., 2008; *Wookey and Helffrich*, 2008].

We collect waveform data from 242 events that occurred in and around South America and the Southern Atlantic Ocean between 2004 and 2009. All events are located at the epicentral distances ranging between 147° and 155° from the Hi-net array stations (Figure 2.2). Total of 47 events (Table 1), out of which 12 events in the QEH (No.1-12 in Table 1) and 35 events in the QWH (No.13-47 in Table 1), were selected applying restrictive data quality criteria based on the correlation coefficient, signal-to-noise ratio (SNR), and visual inspection of waveforms. Event information was taken from the reviewed Bulletin of the International Seismological Centre (ISC), which is manually checked by ISC analysts and relocated. The targeted events have the body wave magnitudes (m_b) between 5.0 and 6.7. All qualified seismograms that were selected for a further study satisfy the following conditions: 1) The correlation coefficient between BC and DF waveforms is larger than 0.6; 2) The SNR of the PKP_{DF} is higher than 2; 3) The PKP_{DF} travel-time curves are clearly identified by eye when all waveforms for an event are aligned with respect to the detected PKP_{BC} phases (Figure 2.3). If the range of the epicentral distance for the PKP_{DF} travel-time curves is too short (under 2°) or include empty spaces (over 1.5°), although the PKP_{DF} travel-time curves were clear, we ruled the event out. Prior to the waveform cross-correlation, all seismograms were band-pass filtered between 0.3 and 2 Hz and 6070 seismograms were finally selected from more than

50,000 seismograms.

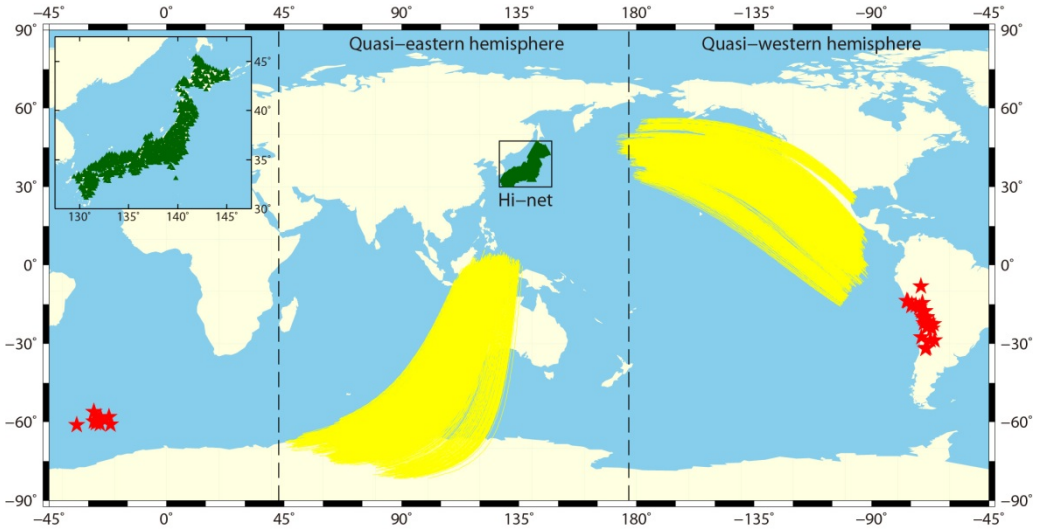

Figure 2.2. Surface projections of PKP_{DF} ray-paths considered in this study. Total of 47 events passed strict quality selection criteria and their corresponding ray-paths are shown in red and yellow. Hi-net array stations (also shown enlarged in inset) are displayed by green triangles. The quasi-hemispheric boundaries (43°E, 177°W) defined by *Tanaka and Hamaguchi* [1997] are represented with dashed lines.

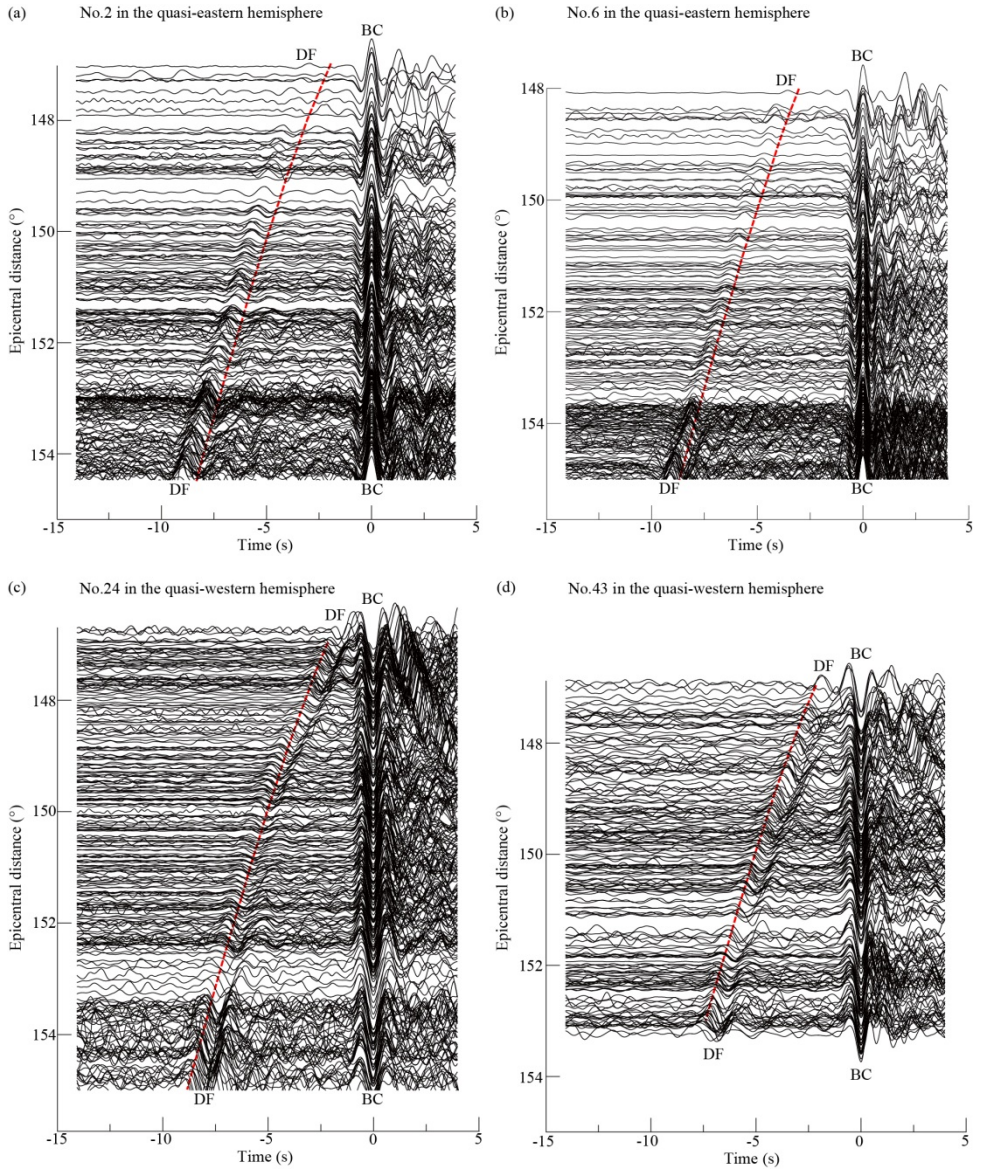

Figure 2.3. Selected teleseismic waveforms recorded on Hi-net stations aligned with respect to the detected PKP_{BC} waves for (a) event "No. 2" and (b) event "No. 6" with ray sampling in the QEH and (c) event "No. 24" and "No. 43" with ray sampling in the QWH of the IC (see Table 1). Red dots are theoretical predictions of PKP_{DF} wave arrivals from ak135 model [*Kennett et al.*, 1995].

Table 1. Event parameters used in this study from the reviewed Bulletin of the ISC.

No	Origin Date	Origin Time (UT)	m_b	Latitude, ˚N	Longitude, ˚E	Depth, km
1	2006-01-02	06:10:48	6.2	-61.0106	-21.6489	10.0
2	2008-07-01	01:54:40	5.6	-58.2510	-21.8078	3.4
3	2004-09-11	21:52:34	5.9	-58.0207	-25.5207	35.6
4	2008-02-10	12:22:03	6.3	-60.7841	-25.5944	10.0
5	2005-08-04	12:11:18	5.7	-59.6285	-25.8459	44.3
6	2008-10-04	07:56:50	5.7	-59.4516	-25.8971	20.6
7	2006-05-29	05:20:38	5.5	-59.6523	-26.3024	37.4
8	2009-04-16	14:57:06	6.0	-60.2882	-27.0291	17.6
9	2007-07-31	02:42:49	5.8	-56.1028	-27.7318	113.3
10	2008-07-30	20:15:12	5.2	-59.7161	-27.8818	136.2
11	2005-09-09	19:55:18	5.7	-56.0067	-27.9467	125.0
12	2006-08-20	03:41:45	6.2	-61.0160	-34.2851	0.5
13	2004-09-07	11:53:04	6.0	-28.5709	-65.8815	22.1
14	2007-11-18	05:40:09	5.6	-22.6479	-66.2655	216.4
15	2005-06-02	10:56:00	5.5	-24.1334	-67.0103	194.9
16	2006-07-08	09:13:01	5.0	-28.6014	-67.4005	142.0
17	2005-11-17	19:26:54	5.9	-22.3676	-67.9421	161.7
18	2007-12-26	23:40:54	5.5	-22.3836	-68.3077	107.6
19	2006-11-14	22:22:12	5.4	-23.3092	-68.3195	109.5
20	2006-06-27	02:07:32	5.3	-22.5086	-68.4005	102.7
21	2004-06-17	01:16:00	5.2	-21.1833	-68.4451	115.4
22	2006-06-27	11:24:36	5.2	-21.2606	-68.4507	124.1
23	2008-01-05	07:29:33	5.5	-22.8861	-68.5037	105.4
24	2007-11-24	05:02:08	5.5	-23.7141	-68.8211	96.3
25	2005-08-14	02:39:39	5.6	-19.7422	-69.0809	114.6
26	2005-09-09	11:26:05	5.7	-31.6236	-69.1411	114.0
27	2008-09-10	16:11:59	5.5	-20.3049	-69.1785	3.9
28	2005-06-13	22:44:32	6.7	-19.9172	-69.2156	111.9
29	2009-05-08	13:44:53	5.6	-32.0330	-69.7032	113.3
30	2005-04-16	22:41:14	5.6	-17.6207	-69.7036	118.8
31	2007-11-14	15:40:49	6.6	-22.3208	-69.7803	33.6
32	2008-02-04	17:01:31	5.9	-20.1855	-69.9476	42.8
33	2007-03-24	19:13:50	5.6	-19.7094	-70.0611	27.7
34	2006-11-20	14:38:28	5.7	-17.6936	-70.1605	41.5

35	2005-07-13	12:06:11	5.5	-17.8565	-70.2123	79.3
36	2006-04-09	20:50:46	5.5	-20.4669	-70.2285	36.2
37	2009-04-17	02:08:09	5.8	-19.5806	-70.5024	28.7
38	2006-08-09	22:36:09	5.5	-14.4277	-70.6862	35.0
39	2004-08-27	00:43:52	5.7	-27.4305	-70.7903	30.6
40	2007-02-07	18:55:00	5.3	-17.7624	-70.9882	65.7
41	2007-07-21	13:27:03	6.1	-08.0859	-71.2071	633.7
42	2008-07-08	09:13:07	5.8	-15.9861	-71.7482	122.6
43	2005-07-26	14:11:34	5.7	-15.3386	-73.0597	109.1
44	2005-05-03	19:11:38	5.5	-14.8785	-74.6701	31.4
45	2007-06-28	08:44:48	5.4	-15.7255	-74.8709	27.9
46	2007-08-18	02:52:36	6.0	-13.8095	-76.2970	33.4
47	2007-08-19	01:22:38	5.8	-13.6101	-76.6104	13.4

Ray-paths in this study almost exclusively sample each quasi-hemisphere because not only the bottoming points of the PKP_{DF} phase are located within each quasi-hemisphere defined by previous studies (see Table 2), but also the corresponding entry and exit points at the ICB are almost entirely confined within a single hemisphere for most of earlier studies [e.g. *Tanaka and Hamaguchi*, 1997; *Creager*, 1999; *Garcia and Souriau*, 2000; *Niu and Wen*, 2001; *Garcia*, 2002; *Oreshin and Vinnik*, 2004; *Irving and Deuss*, 2011] (Table 2). Moreover, the entry, bottoming, and exit points are closely clustered in each quasi-hemisphere. Because we focus on regional variation of velocity in the UIC, the entry and exit points should be approached critically in contrast to most previous studies concerning just the bottoming points. The lateral extent of IC area for selected ray-paths is 31.3° for the QEH and 43.0° for the QWH. At the ICB depth, these ranges correspond to about 665 and 915 km for each hemisphere, respectively.

Table 2. The definition of quasi-hemispherical boundaries from previous studies and ray-sampling points from this study.

Quasi-eastern hemisphere	**Quasi-western hemisphere**	**Reference**
43°E-177°E	177°E-43°E	Tanaka and Hamaguchi [1997]
40°E-160°E	160°E-40°E	Creager [1999]
40°E-160°E	160°E-40°E	Garcia and Souriau [2000]
40°E-180°E	180°E-40°E	Niu and Wen [2001]
60°E-180°E	180°E-60°E	Garcia [2002]
50°E-120°W	120°W-50°E	Oreshin and Vinnik [2004]
14°E-151°W	151°W-14°W	Irving and Deuss [2011]
Range of bottoming points in the QEH	**Range of bottoming points in the QWH**	This study
95.70°E-130.54°E	114.14°W-138.01°W	
Range between entry and exit points	**Range between entry and exit points**	
45.40°E-135.53°E	171.99°E-91.15°W	

3. PKP_{BC}-PKP_{DF} differential travel-times

Since PKP_{DF} and PKP_{BC} phases have similar ray-paths in the uppermost mantle (Figure 2.1a), PKP_{BC}-PKP_{DF} differential travel-times (BC-DF) are only weakly sensitive to event depth and origin time uncertainties. We compared the reviewed ISC Bulletin and the Preliminary Determination of Epicenters (PDE) Bulletin by the National Earthquake Information Center (NEIC) to estimate possible mislocation of earthquakes, and observed that the maximum difference is 33.8 km in depth and 0.2° in epicentral distance. Uncertainties of the theoretical BC-DF travel-times imposed by these maximum values are only 0.03 s taking into account the uncertainty in depth and 0.16 s taking into account the uncertainty in epicentral distance. In addition, the effects from strong heterogeneities near the core-mantle boundary (CMB) could be considered less significant under the assumption that the separation between PKP_{DF} and PKP_{BC} is smaller than a typical heterogeneity wavelength in the D'' layer [e.g. *Shearer and Toy*, 1991; *Bijwaard et al*., 1998; *Lay et al*., 1998; *Bréger et al*., 1999; *Romanowicz et al*., 2003]. Indeed, a study of possible trade-off effects of the lowermost mantle structure and IC anisotropy on BC-DF confirmed that the trends observed in BC-DF residuals cannot be explained exclusively by the D'' structure [*Tkalčić et al*., 2002].

The waveform cross-correlation method was used to identify PKP_{BC} and PKP_{DF} phases and to measure BC-DF [e.g. *Shearer and Toy*, 1991; *Tkalčić et al*., 2002]. The method takes advantage of the fact that the waveforms of those two core phases are similar because of a similar source radiation and the proximity of their paths through the Earth's mantle. Before performing a cross-correlation of PKP_{BC} and PKP_{DF} phases on the large number of Hi-net stations for a single event in an automatic fashion, we pick a clear PKP_{BC} phase manually. This single time then serves as a reference time. The seismogram for the reference pick corresponds to epicentral distance of about 149° to avoid interference with the PKP_{AB}, PKP_{DF} and PKiKP phases that appear closer to PKP_{BC} phase when the epicentral distance approaches 145° on the one or 155° on the other side of the range (Figure 2.1b). We collect the PKP_{BC} phase arrivals from the rest of the seismograms by cross-correlation with the reference PKP_{BC} phase. Another cross-correlation is then performed to detect the PKP_{DF} phase on each seismogram. BC-DF are measured from cross-correlation lag times, the maxima of the cross-correlation function. Lastly, all selected seismograms are visually inspected. According to the reference model ak135 [*Kennett et al*., 1995], PKP_{BC} and PKP_{DF} phases can be observed on the same seismogram for epicentral distances from about 145° to 155°. However, we do not consider data corresponding to the epicentral distances smaller than 147° because PKP_{BC} and

PKP_{DF} arrivals are too close to each other, making the systematic detection of PKP_{DF} phases by cross-correlation less reliable.

A travel-time residual Δt for each seismograms is defined as a difference between $(BC-DF)_{obs}$ - the observed (measured) differential travel-time, and $(BC-DF)_{1D}$ - the theoretical differential travel-time for different spherically symmetric reference Earth models. This can be described by the following equation:

$$\Delta t = (BC-DF)_{obs} - [(BC-DF)_{1D} + (BC-DF)_{ellip}] \quad (1)$$

where $(BC-DF)_{ellip}$ is the Earth's ellipticity correction (not significant, but still taken into account). If the lowermost mantle structure is corrected for, the above equation becomes:

$$\Delta t = (BC-DF)_{obs} - [(BC-DF)_{1D} + (BC-DF)_{ellip} + (BC-DF)_{LM}] \quad (2)$$

where $(BC-DF)_{LM}$ represents contribution from the lowermost mantle. The lowermost mantle contribution will be discussed in more detail in Section 4.5.

4. Results

4.1. Argument against uniform cylindrical anisotropy

PKP_{DF} ray-angles with respect to the Earth's spin axis (conventionally denoted by ξ) for the ray-paths in this study fall between 40.56° and 45.79° in the QEH and 50.42° and 69.83° in the QWH. The values of these angles indicate that all our paths are quasi-equatorial (ξ between 35° and 90°). Assuming that the IC has a uniform cylindrical anisotropy about the Earth's spin axis, the perturbed velocity can be expressed as:

$$\delta Vp = A + B\,cos^2\,\xi + C\,cos^4\,\xi \qquad (3)$$

For ξ varying between 35° and 90°, the equation (3) predicts the range of BC-DF residuals to be about 1.7 s for 3.5% anisotropy (A = 0.018, B = -0.165, C = 0.557 km/s; [*Creager*, 1992]) and 0.4 s for 0.6% anisotropy (A = 0.000, B = 0.012, C = 0.056 km/s; [*Shearer and Toy*, 1991]) (see curves in Figure 2.4). However, ξ corresponding to the selected waveforms in our study is restricted within narrow ranges of about 5° and 19° in each quasi-hemisphere (gray areas in Figure 2.4). It is straightforward to show that the effect of a possible strong uniform cylindrical anisotropy (such as that of 3.5%) is too small to explain the magnitude of the observed BC-DF residuals. More specifically, for these small variations in angle ξ, the corresponding predicted range of residuals for 3.5%

anisotropy is less than 0.5 s in both hemispheres (see the extent of red lines in gray areas of Figure 2.4), while our observed travel-time residuals are much larger (Figure 2.5).

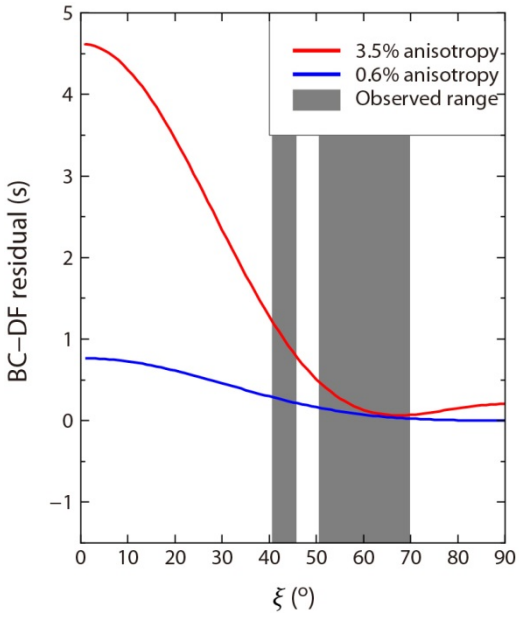

Figure 2.4. Ranges of ξ (the angle between PKP_{DF} and the Earth's rotation axis in the IC) for the waveforms from this study are represented as gray-shaded areas. The theoretical curves of travel-time residuals for a uniform cylindrical anisotropy of 0.6% [*Shearer and Toy*, 1991] and 3.5% [*Creager*, 1992] are plotted in blue and red lines, respectively.

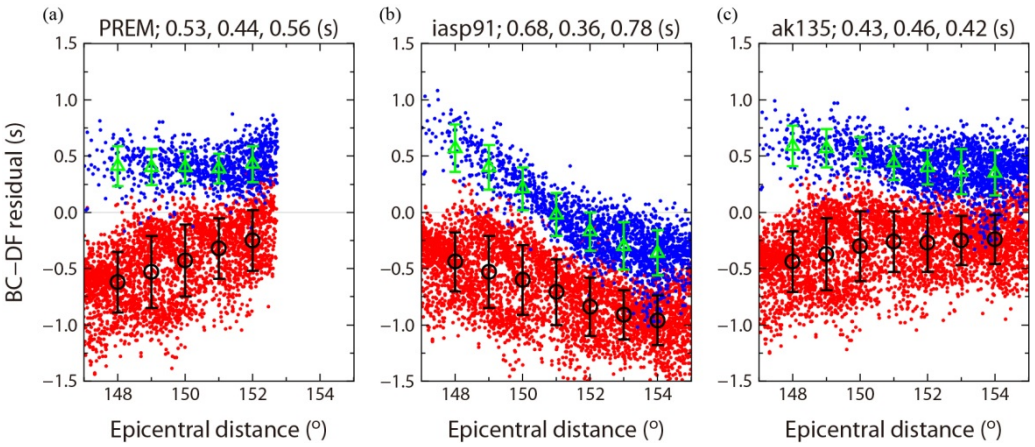

Figure 2.5. Observed BC-DF residuals with respect to three spherically symmetric reference Earth models: (a) PREM [*Dziewonski and Anderson*, 1981], (b) iasp91 [*Kennett and Engdahl*, 1991] and (c) ak135 [*Kennett et al.*, 1995] for the ray-paths sampling in the QEH (blue dots) and the QWH (red dots). The means for the data confined within the interval ±1° are calculated at each whole degree (green triangles for the QEH and black circles for the QWH). Corresponding ±1 standard deviation is shown with vertical bars. RMS values are calculated for the entire dataset, the QEH data only, and the QWH data only, and are shown by the three numbers above each plot.

4.2. Hemispherical dichotomy in the UIC

When the BC-DF residuals for three commonly used reference models (PREM [*Dziewonski and Anderson*, 1981], iasp91 [*Kennett and Engdahl*, 1991], and ak135 [*Kennett et al*., 1995]) are plotted as a function of epicentral distance, these plots show clear distinction between the QEH and the QWH (Figure 2.5). Negative travel-time residuals are robustly observed in the QWH indicating a slower UIC with respect to the 1D Earth reference models. Positive travel-time residuals in the QEH indicate that the P wave velocity in the UIC is faster than the 1D Earth reference models and most observed residuals show positive values except for the iasp91 reference model. The residuals of the QEH with respect to the iasp91 change from being positive to being negative as the epicentral distance increases because the slope of the observed and predicted BC-DF curves is quite different. This difference of the slope is mainly constrained by the velocity structure at the bottom of the outer core as will be shown by a synthetic test described in section 4.3. On the other hand, in case of PREM and ak135, the slope of the BC-DF curves is similar between the observation and prediction for each event (Figure 2.6).

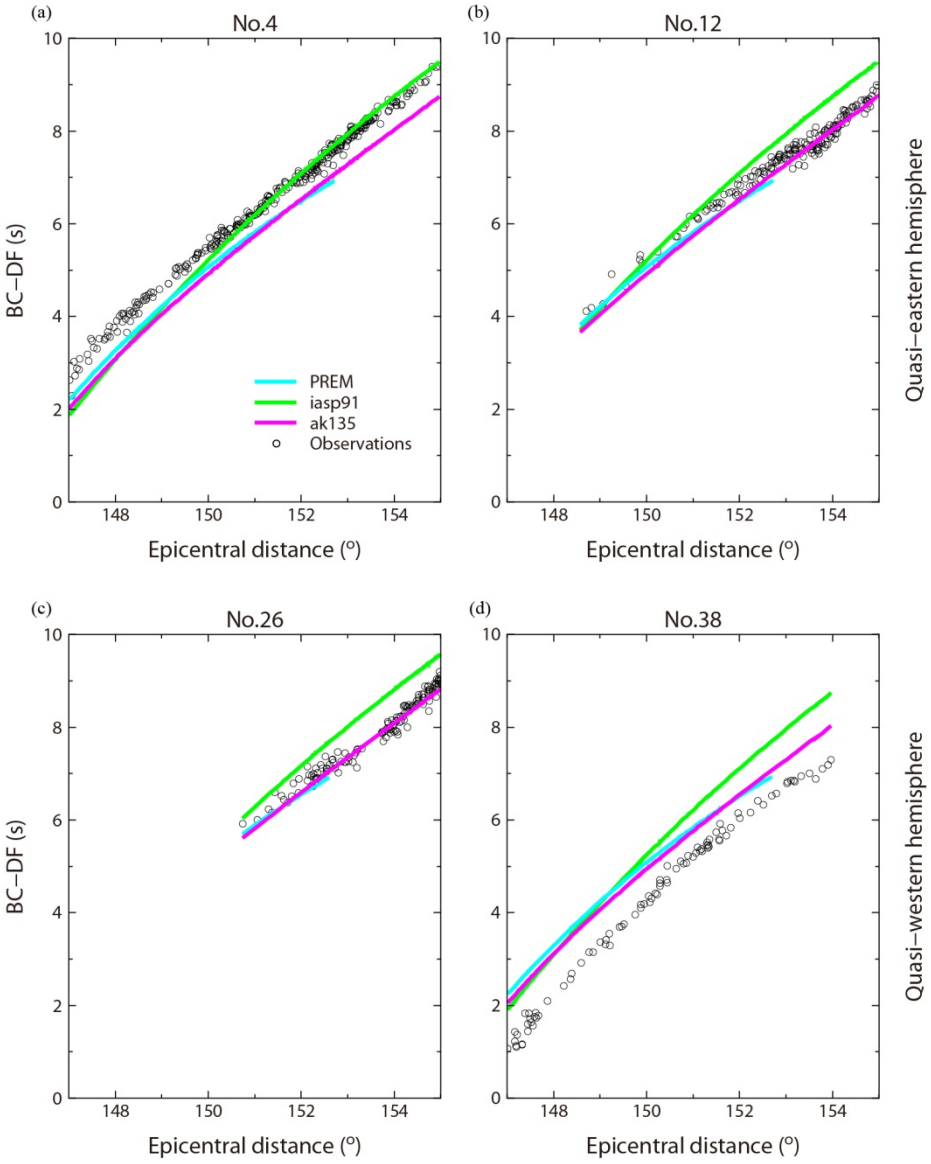

Figure 2.6. Theoretical BC-DF from PREM (cyan line), isap91 (green line), and ak135 models (magenta line) are plotted against the observed BC-DF (black dots) for (a) the event No. 4 and (b) event No. 12 in the QEH, and (c) the event No. 26 and (d) event No. 3 in the QWH. The slopes of the PREM- and ak135-based BC-DF theoretical curves and observations are similar, but they differ for the iasp91 model.

The root-mean-square (RMS) values between the observations and the reference models are 0.53, 0.68 and 0.43 s for PREM, iasp91 and ak135, respectively. Since the slopes of the BC-DF curves between the observation and the prediction from iasp91 model show large deviations, we conclude that ak135 model is more relevant in further modeling of the velocity variations in the UIC. It should not be surprising that ak135 constrains PKP travel-times after some adjustments better than iasp91, as ak135 was a significant improvement from iasp91 as a result of the addition of PKP travel-times. The mean values and standard deviation of the observed BC-DF residuals are +0.41±0.16 s for PREM and +0.42±0.19 s for ak135 in the QEH and −0.46±0.33 s for PREM and −0.31±0.28 s for ak135 in the QWH. These mean values are quite comparable to the results obtained in previous studies [e.g. *Tanaka and Hamaguchi*, 1997; *Niu and Wen*, 2001].

4.3. Lateral variations on regional scales in the UIC

The shift of empirical BC-DF curves for all events (Figure 2.6) suggests that continuous variations of the velocity structure exist on regional scales. These variations could be confirmed at a glance from the distribution of residuals on the entry, bottoming, and exit points in the IC (Figure 2.7). All residuals are spread from −0.33 s to +1.00 s in the QEH and from −1.25 s to +0.46 s in the

QWH. We identify a smooth transition from a slower eastern region to a faster western region in the QEH. Similarly, there is an apparent transition from a slower northern region to a faster southern region in the QWH. Travel-time residuals that are shown with circles in Figure 2.7 are a result of an averaged velocity field within the corresponding ray's Fresnel zone, the value of which determines the PKPDF travel-time. Fresnel zones corresponding to adjacent sampling points cover similar volumes of the UIC, but they also each include a slightly different volume causing a smooth spatial variation in the observed residuals. The maximum radius of the Fresnel zone for a PKPDF phase with a dominant period of 1 s could be up to about 6.9° (148 km at the ICB; see the dashed circle in Figure 2.7) at the epicentral distance of 150° [Calvet et al., 2006]. A lateral extent of the UIC sampled by ray-paths in this study exceeds this radius in both sampling areas (31.3° in the QEH and 43.0° in the QWH).

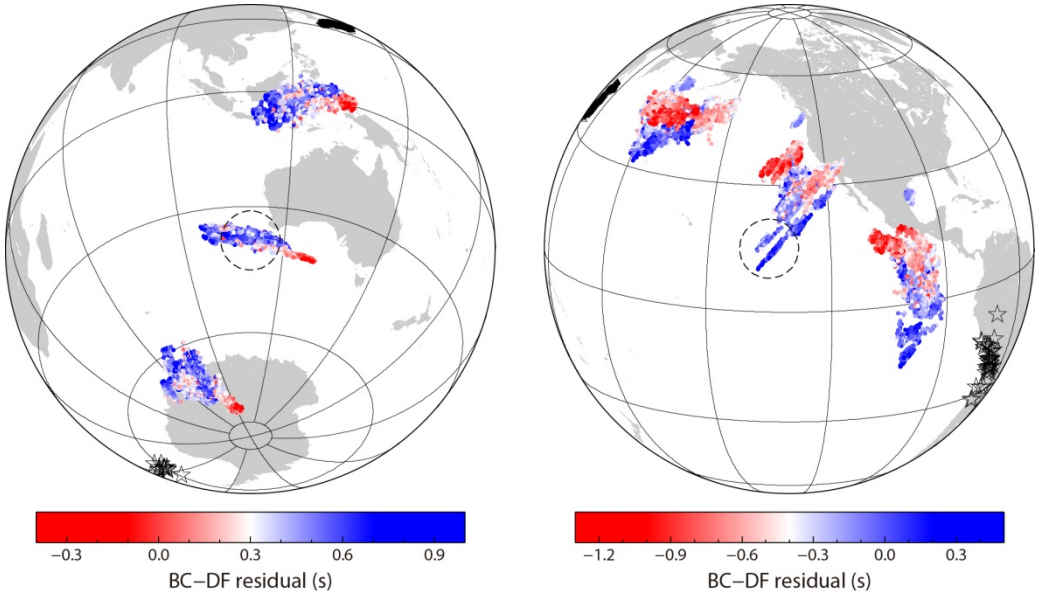

Figure 2.7. Distribution of residuals on the entry, bottoming, and exit points in the IC are plotted in each quasi-hemisphere. Dashed circle indicates the radius of the Fresnel zone for a PKP_{DF} phase with a dominant period of 1 s at the epicentral distance of 150°. Black stars and triangles represent the selected events and Hi-net stations, respectively.

In order to explain the observed shift of BC-DF curves, we perturb IC velocity structure using a grid-search approach, starting from spherically symmetric P-wave velocity models. PREM [*Dziewonski and Anderson*, 1981], iasp91 [*Kennett and Engdahl*, 1991], and ak135 [*Kennett et al*., 1995] are used to represent the mantle and the outer core, while P-wave velocity at the top of the IC is sampled from 10.87 km/s to 11.17 km/s with an interval of 0.01 km/s (Figure 2.8). Velocity structure between the top of the IC and the depth of about 5500 km (350 km below the ICB) is linearly interpolated. The PKP_{DF} phases considered here do not travel through the IC below the depths of about 350 km, which corresponds to the epicentral distances of 155°. Therefore the velocity structure outside these boundaries does not affect the BC-DF.

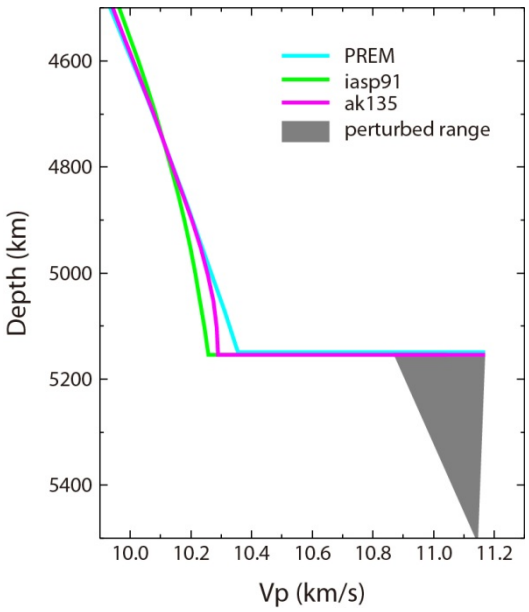

Figure 2.8. Trial models modified from PREM (cyan line), iasp91 (green line) and ak135 (magenta lines) for grid-search. The velocity at the top of the IC was varied from 10.87 km/s to 11.17 km/s with an interval of 0.01 km/s (gray shadow).

The best-fitting models were determined by finding the lowest RMS value between the observed and theoretical BC-DF curves. The starting models are generated from each of the three reference models for each of the 47 selected events. Possible uncertainties due to sampling different event-station pairs within a broad region, event mislocations, site characteristics, different radiation patterns, and different source time functions, are negligible because we estimate a single P-wave velocity model for each event. For simplicity, the best-fitting modification of PREM for an individual event is referred to as mod-PREM and a consistent nomenclature is used for other two reference models (mod-ak135 and mod-iasp91). It is clear that the slopes of the best-fitting BC-DF curves from the forward modeling do not change when different events are compared (Figures 2.9a and 9b for the QEH, and Figures 2.9c and 9d for the QWH as same as Figure 2.5 for comparison). The best-fitting curves for mod-PREM and mod-ak135 show little difference and have similarly low RMS values. Using a bootstrap method, we resampled the observations and performed a grid-search 500 times, to estimate the robustness of the best-fitting models. On average, about 78% of the best-fitting models were reselected (insets in Figure 2.9).

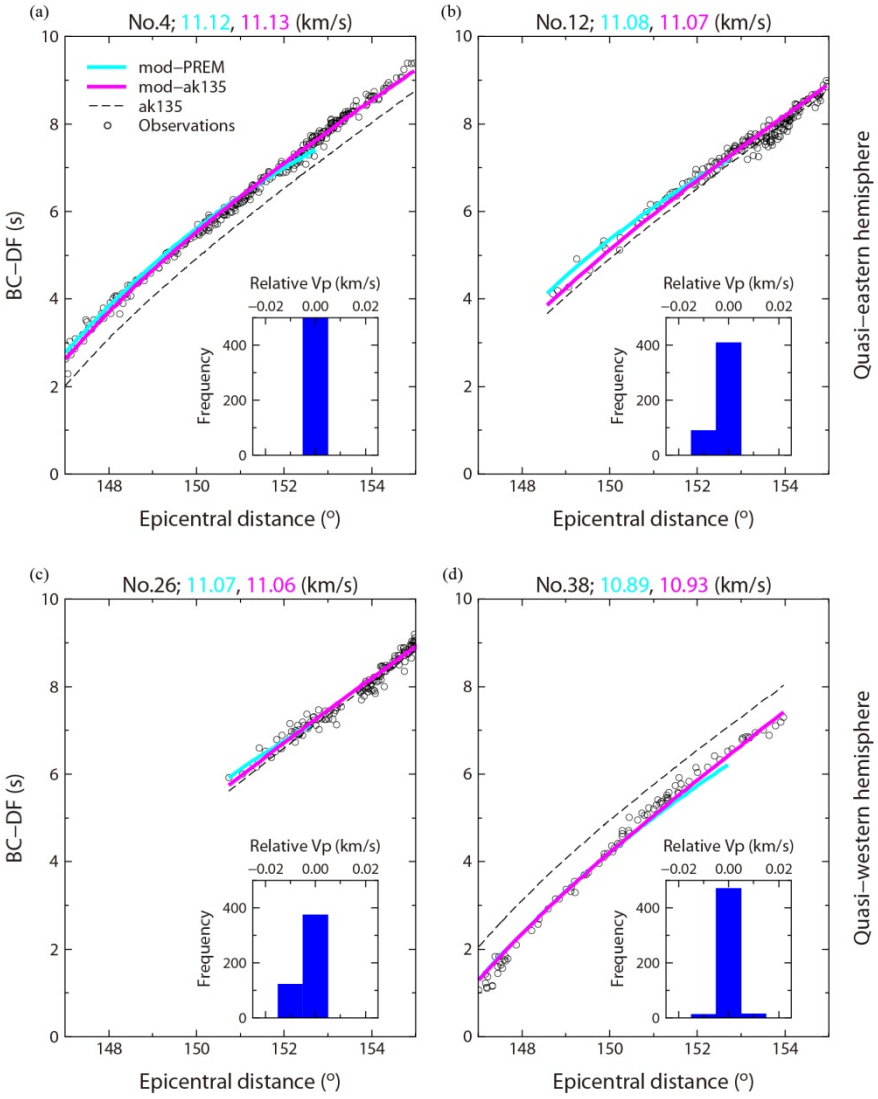

Figure 2.9. Observed (black dots) and theoretical BC-DF curves for ak135 (black dashed line), mod-PREM (cyan line) and mod-ak135 (magenta line) for: (a) event No. 4, (b) event No. 12, (c) event No. 26, and (d) event No. 38 (see also Figure 2.6). The best-fitting velocities at the ICB according to mod-PREM and mod-ak135 are noted above plots. Insets show the bootstrap results as histograms with the total number of models on vertical, and the compressional velocity perturbations on horizontal axes.

For all analyzed events, the RMS value decreased from 0.53 s for PREM to 0.20 s for mod-PREM and from 0.43 s for ak135 to 0.18 s for mod-ak135 (Figure 2.10) and the best-fitting velocity for each event is specified in Table 3. Since each individual path is treated separately, it is not surprising that these values represent significant improvement in velocity structure when compared with the reference models. The RMS values for the QEH and the QWH are 0.14 s and 0.21 s for mod-PREM models and 0.14 s and 0.20 s for mod-ak135 models. At the same time, even the best-fitting models derived from iasp91 do not explain the observations as well as other modified models. A decrease in the residual RMS value for the best-fitting models modified from iasp91 is irrelevant because the BC-DF curves between the observations and the reference model are quite dissimilar as mentioned in the section 4.1. Therefore, we conclude that individual mod-ak135 models and mod-PREM models can explain the observations equally well.

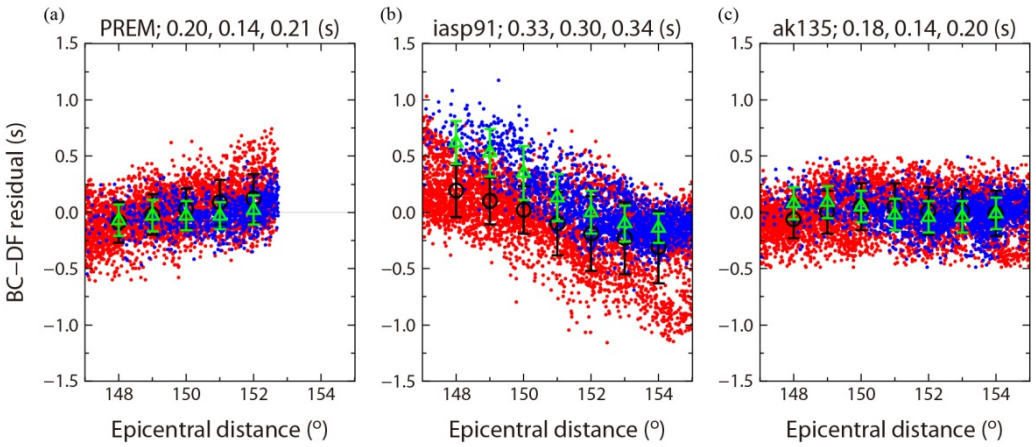

Figure 2.10. BC-DF residuals calculated with respect to the best-fitting models: (a) mod-PREM, (b) mod-iasp91, and (c) mod-ak135 for the QEH (blue dots) and the QWH (red dots). The means for the data confined within the interval ±1° are calculated at each whole degree (green triangles for the QEH and black circles for the QWH). Corresponding ±1 standard deviation is shown with vertical bars. RMS values are calculated for the entire dataset, the QEH data only, and the QWH data only, and are shown by the three numbers above each plot.

For individual mod-ak135 and mod-PREM models, the best-fitting P-wave velocities at the top of the IC vary between 11.07 and 11.13 km/s (about +0.3~+0.8% with respect to ak135) and between 11.07 and 11.15 km/s (about +0.4~+1.1% with respect to PREM) in the QEH. The velocities vary between 10.91 and 11.06 km/s (about −1.2~+0.2% with respect to ak135) and between 10.87 and 11.07 km/s (about −1.4~+0.3% with respect to PREM) in the QWH (Figure 2.11). In other words, the velocity in the UIC is perturbed in 2.0-2.5% on a global scale, considering ak135 and PREM. Moreover, on shorter spatial scales, the maximum velocity perturbation is about 0.5-0.7% in the QEH and 1.4-1.7% in the QWH even for an equatorial path with narrow range (Figure 2.12). These amplitudes are significant in comparison with the results from the previous studies, especially in the context of the proposed cylindrical anisotropy in the IC ranging from values below 1% to up to about 4%.

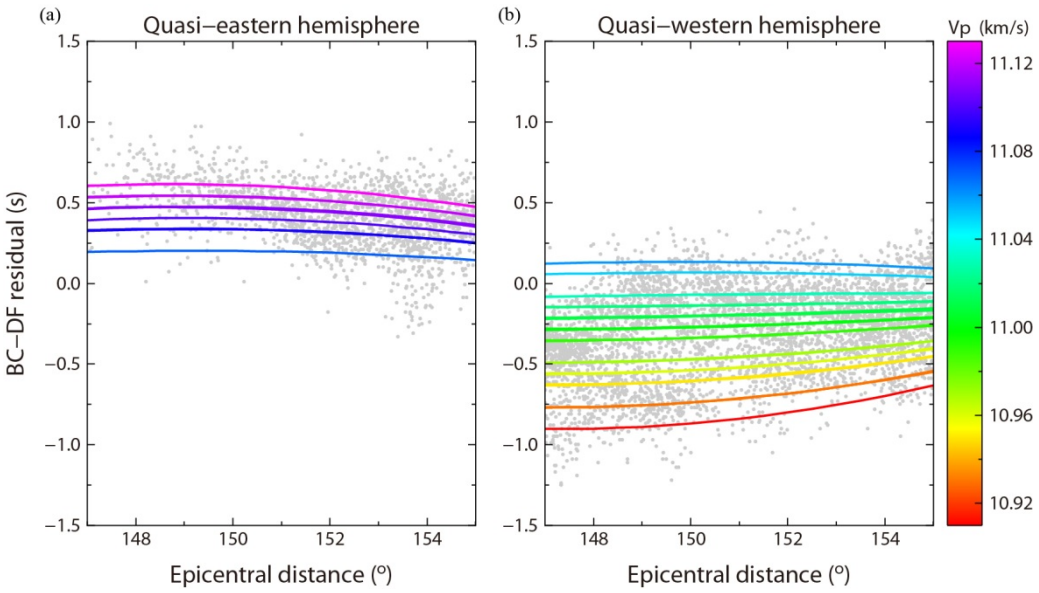

Figure 2.11. Variation of the theoretical BC-DF residuals for 47 events is shown in colors corresponding to best-fitting velocities of mod-ak135 for: (a) the QEH and (b) the QWH. Observed BC-DF residuals with respect to ak135 (same as in Figure 2.5c) are plotted with light gray dots.

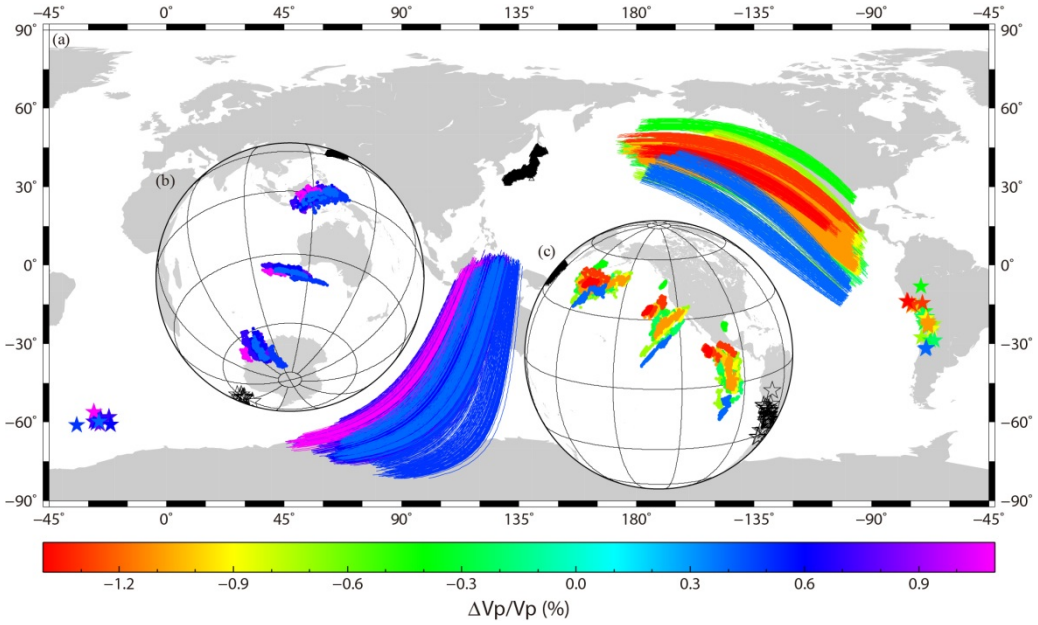

Figure 2.12. (a) Surface projections of great-circle ray-paths of PKPDF in the IC from this study. Colors represent the best-fitting P-wave velocity perturbation from PREM (defining mod-PREM). Stars and triangles represent the selected events and Hi-net stations, respectively. (b) The entry, bottoming and exit points of PKPDF in the IC are plotted in the QEH using the same colors as in (a). (c) Same as (b) but for the QWH.

The best-fitting velocity in Figure 2.12 represents the averaged velocity through a whole ray-path from an entry to an exit point, not an independent velocity at the entry, bottoming, and exit points. Since not all Hi-net stations are aligned along the same great circle path from the event, PKP ray-paths are not all in the same plane and hence they are not projected onto the same great circle. However, azimuthal variations of the stations are relatively small: from 5.81° to 15.54° (mean value is 13.30°) for the events sampling the IC in the QEH and from 4.54° to 18.42° (mean value is 10.87°) for the events sampling the IC in the QWH. We provide averaged 1D velocity models since the number of station-event pairs is still insufficient to constrain more complex modeling approaches. Our study as it stands provides positive proof for the existence of regional velocity variation in the UIC. Velocity structure of the UIC is likely more complicated than that obtained by conventional approaches in which only bottoming points are considered using the angle ξ. The structures at the ICB entry and exit points should have a significant effect on travel-times of PKP_{DF} waves.

4.4. Possible effects from outer core structure

One possibility that has to be excluded before concluding that the bulk of

travel-time anomalies can be attributed to the UIC structure is that the observed travel-time variations are affected by the structure in the outer core. We conduct several synthetic tests to the effects due to velocity perturbations in the outer and the inner core. The velocity in test models based on PREM is changed in the lowermost part of the outer core and the top of the IC. More precisely, the velocity structure between the depth of about 4470 km (680 km above the ICB) and the bottom of the outer core as well as the velocity structure from the top of the IC and the depth of about 5500 km (350 km below the ICB) were linearly interpolated (Figure 2.13a). On the one hand, the depth of 680 km above the ICB marks the upper bound of the depths sampled by the PKP_{BC} phases in our study as it corresponds to the epicentral distances of 145°. On the other hand, the PKP_{DF} phases considered here do not travel through the IC below the depths of about 350 km, which corresponds to the epicentral distances of 155°. Therefore the velocity structure outside these boundaries does not affect the BC-DF.

The most remarkable result of synthetic tests is that when the velocity at the top of the IC is altered (solid and dashed red lines in Figure 2.13a) keeping the velocity in the outer core fixed to PREM values (dotted line), the predicted curves of BC-DF simply shift along the travel-time axis without significant

alterations in the slope (Figure 2.13b). If, however, the velocity at the bottom of the outer core is altered (solid and dashed blue lines), while the velocity in the IC is kept the same (PREM; dotted line), the slope of the predicted curves of BC-DF changes, and the velocity gradient in the outer core affects the location of the c-cusp (Figure 2.13b). The observed travel-time curves for all earthquakes selected in this study regardless of their location show similar slopes to that of ak135 and PREM, but their absolute values vary. This observation, according to our synthetic tests and assuming that reference Earth models provide reasonably good global average, indicates that outer core structure plays less important role in affecting travel-times of PKP waves than structure in the UIC.

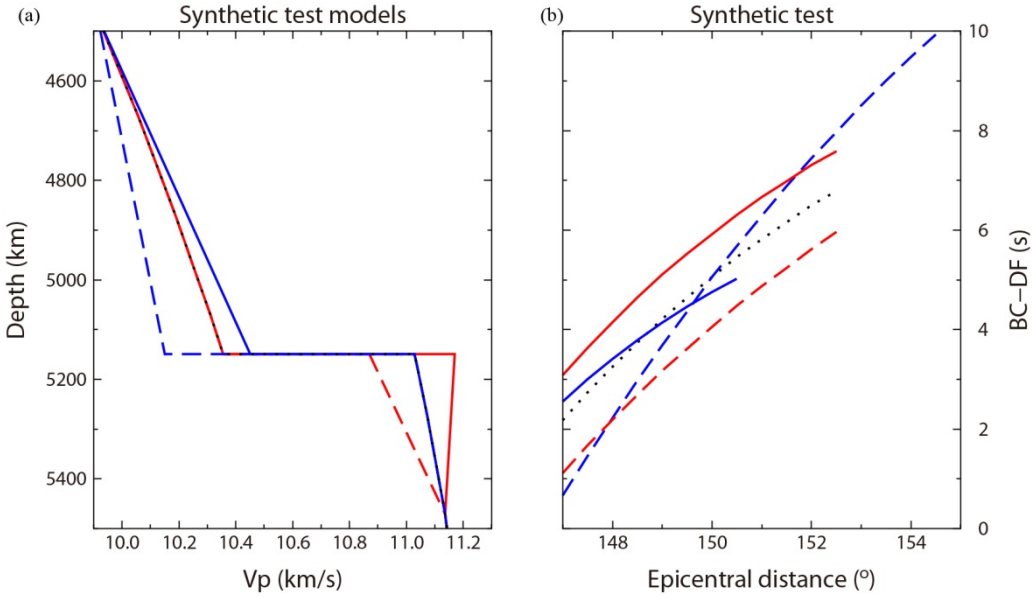

Figure 2.13. Synthetic tests illustrating how changes in velocity profiles in the outer (blue line) and the inner core (red lines) affect theoretical BC-DF curves. (a) In the first test, the velocity profile in the outer core is changed (from a dashed to a solid blue line), while the profile in the IC is fixed to PREM values (dotted line). In the second test, the velocity profile in the IC is changed (from a dashed to a solid red line), while the profile in the outer core is fixed to PREM values (dotted line). (b) The BC-DF curves resulting from the profiles shown in (a) with same color and line style.

Traditionally, the Earth's outer core is considered well-mixed (homogeneous relative to the passage of body waves) due to vigorous convection. Although several researches considered radial inhomogeneity at the top or the bottom of the outer core, it is still regarded laterally uniform [e.g. *Stevenson*, 1987; *Souriau and Poupinet*, 1991; *Romanowicz et al.*, 2003; *Souriau et al*., 2003; *Tanaka*, 2004; 2007; *Ishii and Dziewonski*, 2005; *Zou et al*., 2008]. If velocity structure of the outer core is indeed uniform laterally, the observed difference in the empirical travel-time curves considered here is best explained by lateral variations in IC velocity structure because the travel-times of PKP_{BC} and PKP_{DF} ray-paths are equally affected by outer core velocity structure and the slope of the empirical travel-time curves stay unchanged.

It should be noted that *Yu et al*. [2005] suggested two different P-wave velocity models at the bottom of the outer core for each quasi-hemisphere. According to their study, the QEH model, E1, has a PREM-like velocity structure while the QWH model, W2, has a lower velocity than PREM and a bit higher than ak135 in the bottom of the outer core (Figure 2.14a). Figure 2.14b shows 1 second difference between the E1 (blue) and W2 (red) models, which we confirm is mostly due to UIC structure. Namely, if we adhere to the ak135 velocity profile in the outer core, but change it at the ICB according to W2 and E1 models (two

magenta lines), it becomes clear that BC-DF are not substantially affected by this dichotomy (Figure 2.14b). The difference in velocity structure between PREM and ak135 models at the bottom of the outer core (Figure 2.9) or among the models shown in Figure 2.14 does not yield significant difference in the slopes of the BC-DF curves. Other plausible velocity variations (such that other dataset fits are not significantly reduced) at the bottom of the outer core would only have a minimal effect. Therefore it appears most likely that regional variations of P-wave velocity in the UIC have the most dominant effect on the observed empirical curves of BC-DF.

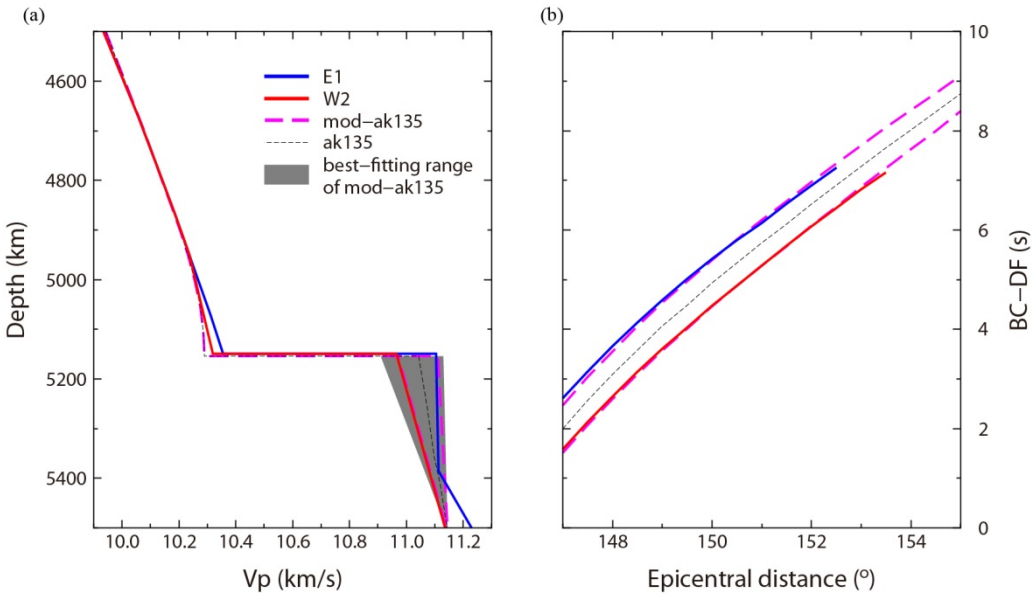

Figure 2.14. (a) Different velocity profiles for the QEH and the QWH: ak135 (dashed black line), E1 (blue line), W2 (red line) [*Yu and Wen*, 2006] and two profiles of mod-ak135 (dashed magenta lines) showing similar velocity at the ICB with respect to E1 and W2. The range of best-fitting mod-ak135 models for the events analyzed in this study is shaded with gray. The velocities at the ICB range from 10.91 to 11.13 km/s. (b) Theoretical BC-DF curves from the models shown in (a) with same color and line style.

4.5. Possible effects from mantle structure

Most previous studies make an assumption that PKP_{DF} and PKP_{BC} waves transit the lowermost mantle in a way that their differential travel-times are not significantly affected by heterogeneous structure. This assumption is valid in the upper mantle where the ray-paths are less separated. However, various scales of heterogeneities in the lowermost mantle have been reported [e.g., *Haddon and Cleary*, 1974; *Bataille and Flatte*, 1988; *Wysession*, 1996; *Su and Dziewonski*, 1997; *Garnero*, 2000; *Dziewonski et al*., 2010]. These anomalies can influence travel-times of PKP phases [e.g. *Bréger et al*., 2000; *Tkalčić et al*, 2002; *Ishii et al*., 2002; *Romanowicz et al.*, 2003; *Tkalčić*, 2010]. The distance between piercing points of PKP_{BC} and PKP_{DF} waves at the CMB varies from about 263 km (4.3°) to about 474 km (7.8°) for the epicentral distance range 147°-155° considered in this study (Figure 2.15a). Thus it is possible and likely that the two PKP phases will pass through quite different velocity field.

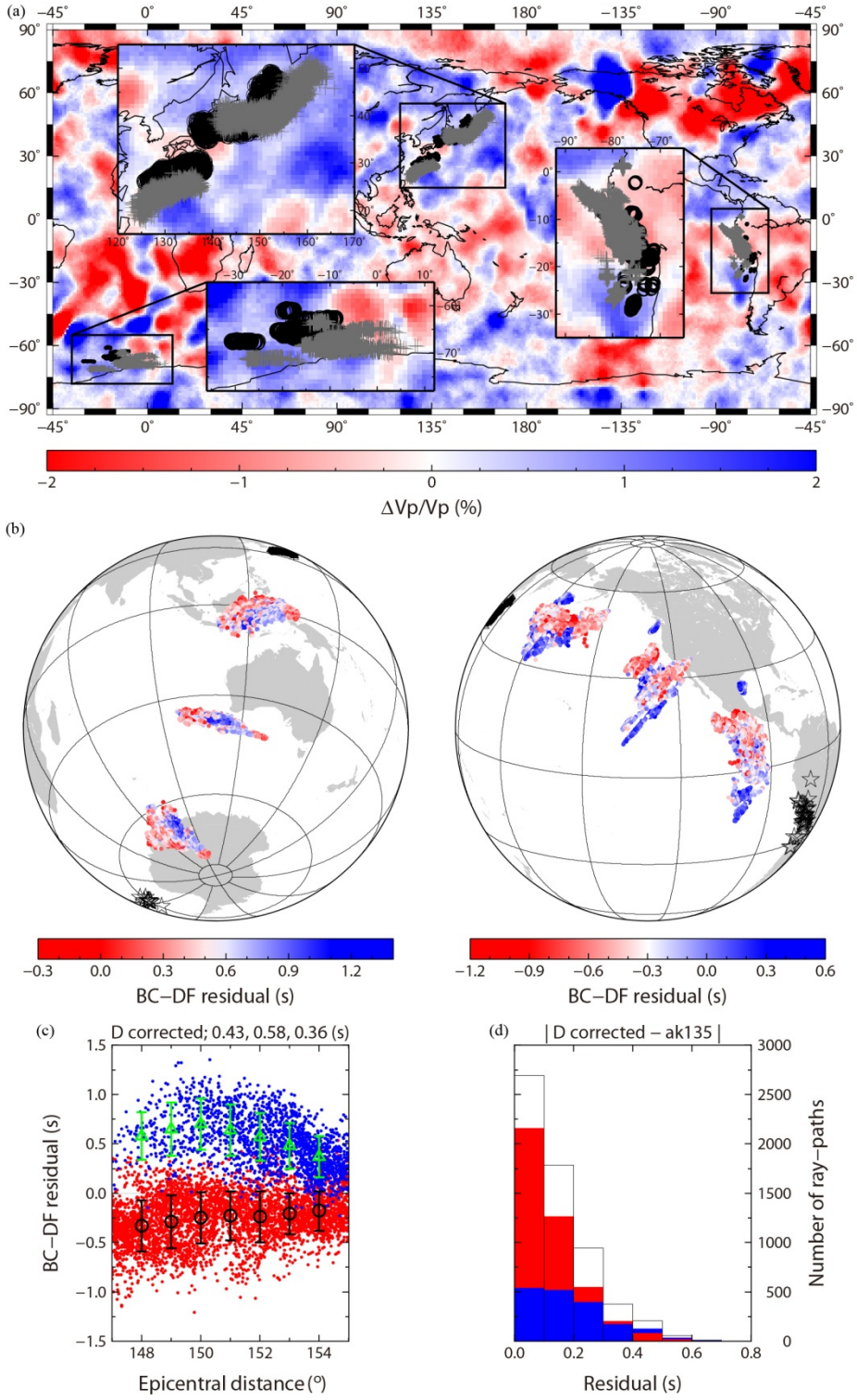
(a)
ΔVp/Vp (%)
(b)
BC–DF residual (s)
BC–DF residual (s)
(c)
D corrected; 0.43, 0.58, 0.36 (s)
BC–DF residual (s)
Epicentral distance (°)
(d)
| D corrected – ak135 |
Number of ray–paths
Residual (s)

Figure 2.15. (a) The entry and exit points of PKP_{BC} (gray crosses) and PKP_{DF} (black circles) ray-paths at the CMB plotted with the *Young et al.*, [2013] tomography model in the background. (b) Distribution of residuals on the entry, bottoming, and exit points in the IC are plotted in each quasi-hemisphere. Black stars and triangles represent the selected events and Hi-net stations, respectively. (c) D''-corrected BC-DF residuals with respect to ak135, plotted in the same way as in Figure 2.5c. (d) Histogram of the absolute difference (in seconds) between the BC-DF travel-times corrected for D'' structure and travel-times predicted by the ak135 model in the QEH (blue bar), QWH (red bar) and their global sum (white bar).

Different tomographic models disagree most strongly in the lowermost mantle, and the disagreements increase as the reported resolvable scale length decreases. Furthermore, the power heterogeneity spectrum of P-wave velocity in the lowermost mantle estimated from previous tomography studies [e.g. *Obayashi and Fukao,* 1997; *Bijwaard et al*., 1998; *Kárason and van der Hilst*, 2001; *Tkalčić et al*., 2002; *Li et al*., 2008; *Dziewonski et al*., 2010; *Soldati et al*., 2012] is typically such that the P-wave velocity variations are under ±1%. There are rare exceptions, such as the study of *Garcia et al*. (2009) according to which the RMS velocity perturbations in the D'' layer are 1.2%. A subjective choice of regularization is a possible cause for differences among travel time tomography models and the underestimate of the heterogeneity power. A recent tomography study of *Young et al*. [2013], in which the inversion is void of explicit regularization, shows a significant increase in the heterogeneity spectrum strength and a visible shift toward shorter spatial scales of heterogeneity in some areas of the lowermost mantle. This tomography model was derived using an extensive dataset of different PKP ray-paths from those that are utilized here, and, importantly, it is characterized by a good spatial coverage in the areas of the lowermost mantle critical for our consideration here, which is confirmed through resolution tests. Furthermore, the tomography model was critically constrained by the addition of PcP-P travel-times that are sensitive to lowermost

mantle structure. Therefore, in order to examine possible contribution to BC-DF by lowermost mantle structure (D'' structure), the model of *Young et al*. [2013] was used to correct our data (Figure 2.15a).

We first recalculate the BC-DF residuals correcting for structure from the *Young et al*. [2013] tomography model. The distribution of residuals on the entry, bottoming, and exit points is plotted in Figure 2.15b and c in the same way as it was done in Fig 7. The BC-DF residuals show a spread from −0.23 s to +1.35 s in the QEH and −1.21 s to +0.53 s in the QWH (Figure 2.15b). The mean values and standard deviation of the D''-corrected residuals are +0.67±0.29 s for PREM and +0.51±0.26 s for ak135 in the QEH and −0.17±0.27 s for PREM and −0.25±0.25 s for ak135 in the QWH. The RMS values for the total, QEH and QWH are 0.43, 0.58 and 0.36 s as against 0.43, 0.46 and 0.42 s for the case of using only ak135 model (Figure 2.15c and Figure 2.5c). These quantitative changes show that the residuals are not only larger but also its range is broadened for the QEH while the opposite is true for the QWH. However, a distinct presence of, and a smooth transition between slow and fast regions can still be discerned in each quasi-hemisphere.

Absolute values of the BC-DF difference between ak135 and D''-corrected

model fall into the 0.0-0.3 s range for more than 89% of the paths (Figure 2.15d) which suggests that the lowermost mantle structure does not have a critical effect on BC-DF in this study. Theoretical maxima for BC-DF residuals with ±1 and ±2% P-wave velocity anomalies in the lowermost 300 km of the mantle are ±1.03 s and ±2.06 s. This means that the travel-times of PKP phases could in theory be significantly affected by the lowermost mantle structure in certain regions. If such data are obtained from individual event-station pairs, it presents a challenge to separate the lowermost mantle from the IC effects. On the other hand, PKP data recorded on dense arrays and/or a group of adjacent events will lend themselves to much less ambiguous interpretation, still resting on an assumption that the separation between piercing points at the CMB is smaller than dominant length-scales of anomalies in the lowermost mantle.

We perform forward modeling to quantitatively compare effects on BC-DF residuals due to D'' structure for each event. The D''-corrected best-fitting P-wave velocities at the top of the IC vary between 11.08 and 11.17 km/s (about +0.3~+1.2% with respect to ak135) and between 11.08 and 11.17 km/s (about +0.5~+1.3% with respect to PREM) in the QEH. The P-wave velocities vary between 10.95 and 11.06 km/s (about −0.8% to +0.2% with respect to ak135) and between 10.93 and 11.06 km/s (about −0.9% to +0.3% with respect to

PREM) in the QWH (Figure 2.16). The range of variation for the best fitting P-wave velocity at the top of the IC increased in the QEH and decreased in the QWH in comparison with the forward modeling that did not contain D''-correction (Figure 2.12). However, an important observation is that the velocity of the UIC shows similar variation, whether we consider the D'' effect or not (Table 3). The amplitude of variations in P-wave velocity is 0.5-0.7% or 0.8-0.9% with D''-correction in the QEH and 1.4-1.7% or 1.0-1.2% with D''-correction in the QWH. Correcting for lowermost mantle structure makes the difference between the two hemispheres less sharp, but does not remove travel-time anomalies from our dataset. Thus, although the heterogeneities in D'' are an important contributor to travel-time variations, they cannot explain the observed significant variations of BC-DF in our study.

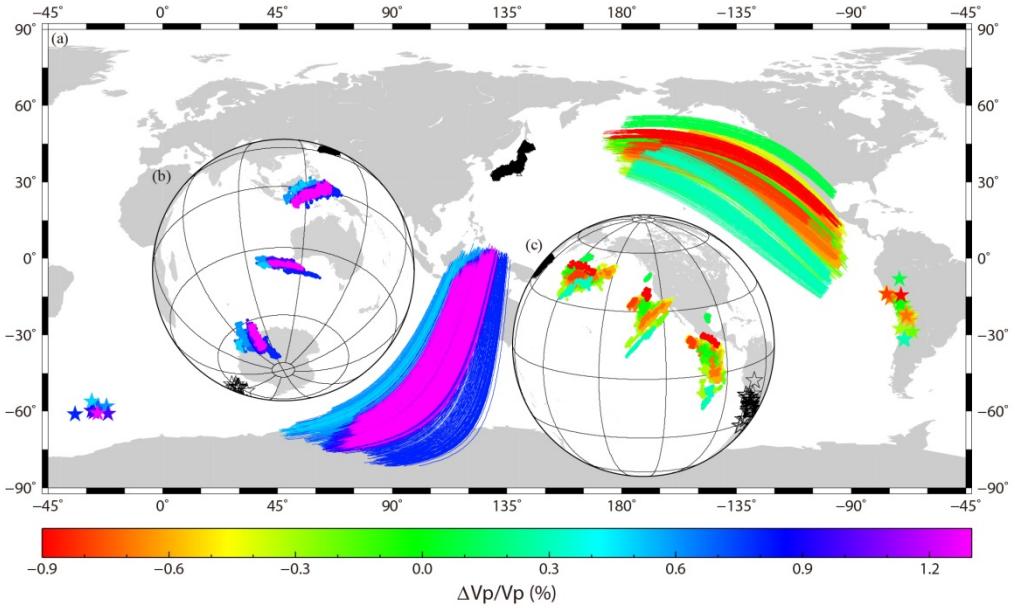

Figure 2.16. (a) Surface projections of great-circle ray-paths of PKPDF in the IC from this study. Colors represent the D''-corrected best-fitting P-wave velocity perturbation from PREM (defining mod-PREM). Stars and triangles represent the selected events and Hi-net stations, respectively. (b) The entry, bottoming and exit points of PKPDF in the IC are plotted in the QEH using the same colors as in (a). (c) Same as (b) but for the QWH.

Table 3. Best-fitting velocities from forward modeling

No	mod-PREM[a]		mod-ak135[b]	
	V_p[c]	V_p for D”-corrected[d]	V_p	V_p for D”-corrected
1	11.09	11.14	11.09	11.14
2	11.10	11.09	11.11	11.09
3	11.11	11.11	11.12	11.11
4	11.12	11.17	11.13	11.17
5	11.07	11.10	11.09	11.10
6	11.09	11.11	11.10	11.11
7	11.09	11.11	11.11	11.11
8	11.11	11.14	11.12	11.14
9	11.15	11.11	11.13	11.11
10	11.11	11.13	11.11	11.12
11	11.13	11.08	11.09	11.08
12	11.08	11.12	11.07	11.12
13	11.01	11.01	11.03	11.02
14	10.95	10.98	11.00	10.99
15	10.93	10.96	10.99	10.97
16	10.99	10.99	11.01	10.99
17	10.95	10.98	10.99	11.00
18	10.91	10.96	10.97	10.97
19	10.91	10.96	10.95	10.97
20	10.91	10.96	10.97	10.99
21	10.93	10.97	10.97	10.97
22	10.91	10.95	10.96	10.97
23	10.91	10.96	10.96	10.98
24	10.99	11.01	11.01	11.01
25	10.97	10.99	10.99	11.01
26	11.07	11.06	11.06	11.06
27	10.97	10.99	10.99	11.00
28	10.93	10.99	10.96	10.99
29	10.97	11.00	11.00	11.01
30	11.07	11.05	11.05	11.06
31	10.99	10.99	11.01	11.00
32	10.99	11.01	11.01	11.02
33	10.97	11.00	11.01	11.01
34	10.99	11.01	11.02	11.02

35	10.99	11.02	11.02	11.03
36	10.97	11.00	11.00	11.01
37	11.01	11.02	11.02	11.03
38	10.89	10.93	10.93	10.95
39	10.95	10.99	11.02	11.01
40	11.00	11.03	11.03	11.04
41	10.98	11.04	11.01	11.05
42	10.97	11.01	11.00	11.02
43	10.92	10.97	10.95	10.99
44	10.89	10.96	10.93	10.97
45	10.91	10.95	10.95	10.97
46	10.87	10.94	10.91	10.96
47	10.89	10.97	10.93	10.98

[a, b] The modification of PREM (ak135) best-fitting the observed BC-DF for an individual event (same number as Table 1). The velocity structure is based on PREM (ak135) except between the top of the IC and the depth of about 5500 km (350 km below the ICB). For grid-search, P-wave velocity at the ICB was sampled from 10.87 km/s to 11.17 km/s with an interval of 0.01 km/s and the velocity structure for 350 km below the ICB was linearly interpolated from the sampled Vp.

[c, d] The P-wave velocity at the ICB from the best-fitting model for the observed BC-DF and for the BC-DF considered an effect by the lowermost mantle anomalies.

5. Discussion

5.1. Radial velocity structure in the UIC

Our modified models contain linearly interpolated velocity structure below the ICB similar to all three Earth reference models considered. However, some researches reported gradient transition in velocity or layered structures in the UIC [e.g., *Yu and Wen*, 2006; *Kazama et al*., 2008].

E1 and W2 [*Yu and Wen*, 2006] show different velocity structures not only in the bottom of the outer core but also in the UIC for each quasi-hemisphere (Figure 2.14a). Contrary to W2 that has a simple velocity structure in the IC (such as the case in our modified models), E1 has a sharp increase in the velocity gradient at 235 km beneath the ICB, which results in a changing slope of the BC-DF curves beyond the epicentral distances of 151°. However the BC-DF curves with respect to mod-PREM and mod-ak135 in the QEH show little difference around the epicentral distance of 151° (Figure 2.14b). Considering more than ±0.5 s deviation in the observed residuals, the changed gradients of the velocity structure are not significant.

Another BC-DF observation indicating regional complexity was also reported

for the QWH by *Kazama et al*. [2008]. In contrast to a simple W2 model, their study showed more complex velocity structure for depth ranges 200-250 km, 250-300 km and 300-350 km below the ICB. We also calculate the theoretical BC-DF from their model. In theory, a layered velocity structure causes discontinuous BC-DF curve, but their model does not produce significantly different effect then one of mod-PREM featured in Figure 2.17. We see no evidence for a discontinuous structure in the observed waveforms. In general, BC-DF curves cannot be explained by the complex model reported in *Kazama et al*. [2008] except for few events collocated with 3 events from their work.

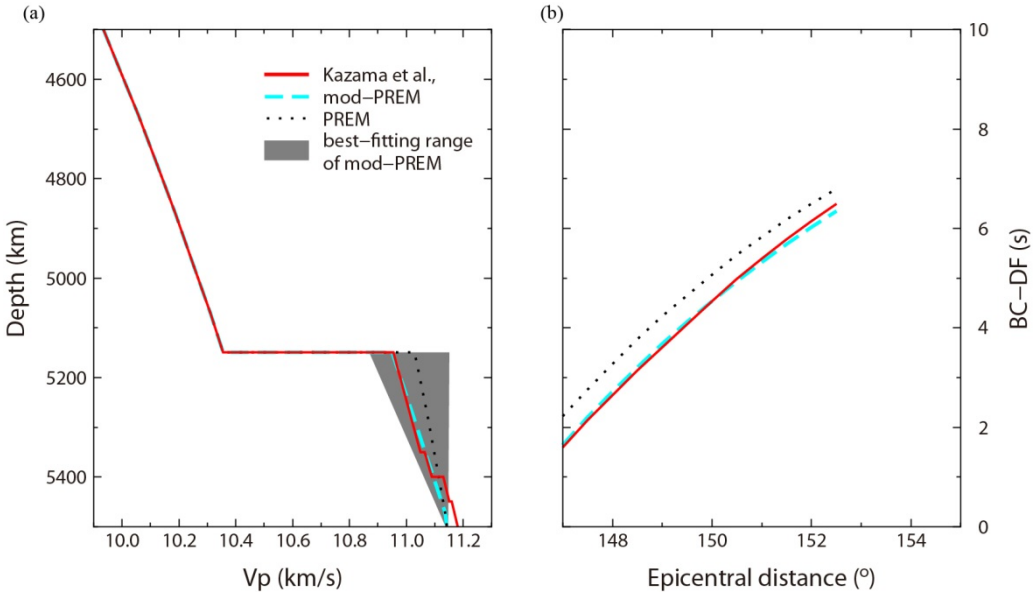

Figure 2.17. (a) Different velocity profiles for the QWH: PREM (black dotted line), the velocity model of *Kazama et al*., [2008] (red line) and one profile of mod-PREM (dashed cyan line) showing similar velocity at the ICB with respect to the profile of *Kazama et al*., [2008]. The range of best fitting mod-PREM models for the events analyzed in this study is shaded with gray. The velocities at the ICB range from 10.87 to 11.15 km/s. (b) Theoretical BC-DF curves from the models shown in (a) with the same color and line style.

The above difference in interpretation might stem from the fact that some of the existing models of IC radial structure have likely been obtained by gathering individual event-station pairs with different entry and exit points in the hemispheres or regions roughly defined by bottoming points of PKP_{DF} wave. Some large residuals influencing a construction of alternative models could be caused by structure of the lowermost mantle or the existence of lateral variations in isotropic velocity in the UIC. However, considering that deviation of ±0.5s or more around the mean is fairly common in the observed BC-DF curves, many non-unique solutions are possible. There will be no significant difference between step-like (discontinuous) and radially-smooth velocity models (interpolated linearly below the ICB using various Earth reference models). Since there is a lack of evidence in the waveforms for a step-like (discontinuous) structure, we argue that mod-ak135 and mod-PREM models present a plausible interpretation.

5.2. Lateral variations in isotropic velocity in the UIC

Despite the fact that many studies have focused on its velocity structure, little is still known about regional variations of IC elastic properties. Part of the problem has been sparse ray-path coverage and the lack of continuous spatial

sampling on regional scales (several hundred km) within the IC. While it was possible to collect a dataset of differential travel-times of core-sensitive seismic phases over a range of epicentral distances from a large number of events [e.g. *Niu and Wen*, 2001; *Tkalčić et al*., 2002; *Yu et al*., 2005; *Garcia et al*., 2006; *Waszek and Deuss*, 2011], it has not yet been possible to collect these measurements from a single event, and use them in a similar fashion in which the travel-time data are used in reflection seismology. However, the establishment of dense permanent arrays with regional-scale apertures has opened a new era in the deep Earth seismology and some of its obvious pay-offs are seen in this study.

Sharp velocity gradients in lateral and radial direction in the UIC have been inferred before beneath Central America [e.g. *Creager*, 1997] and beneath the Indian Ocean [*Stroujkova and Cormier*, 2004]. Our results suggest that these regional variations in the isotropic velocity structure at the UIC are more widespread than what we have previously been able to infer. At this point, it is difficult to speculate if a larger magnitude variation inferred for the QWH has any geodynamical meaning because the number of sampling is different and its spatial distribution is restricted for both hemispheres. Although the difference in maximum amplitude of lateral perturbations of P-wave velocity between the

two hemispheres is reduced after the lowermost mantle corrections are applied, we note that these corrections are still not perfect. They come from a model which assumes that BC-DF data that participate in the model construction, though augmented with other types of data, are affected by exclusively mantle structure. Ideally, the lowermost mantle P-wave velocity model would be constructed from mantle-sensitive data only, however at present, this is not possible as spatial coverage of the existing PcP-P waveform-correlated data is limited. It should also be noted that some extremely thin layers of large P-wave velocity perturbations in the lowermost mantle have been documented through waveform modeling (ultra-low velocity zones), but their thickness and spatial scales are beyond the resolution limit of tomographic imaging. Last but not least, the effects imposed by mantle structure will be fully understood only when they are quantitatively assessed with full waveform modeling. If it can be demonstrated from independent observations that the magnitude of velocity variation in the QWH is indeed stronger than in the QEH, then this, combined with robust observations from body waves and normal modes that the QWH is also slower, might provide important clues on melting and freezing processes. As of now, melting and freezing processes could both be invoked to explain velocity differences in both hemispheres [*Deguen et al.*, 2007].

Since our PKP_{DF} rays have mutually similar angles with respect to the spin axis of the Earth, significant variations of the BC-DF observed in our study cannot be explained with a model of uniform cylindrical anisotropy of the IC. Our data strongly suggest that small-scale regional variations (from the observed variation in empirical BC-DF curves) may be superimposed on a large-scale hemispherical pattern in isotropic velocity (from robust observations that one hemisphere is faster than another). Variations in convection and heat flux in the outer core are sources of heat transfer variations across the ICB, which influences IC growth and crystal alignment [e.g., *Yoshida et al*., 1996]. Regional variations in isotropic velocity in the IC have been suggested through the observation of variations in crystal alignment [*Creager*, 1997], texture [*Stroujkova and Cormier*, 2004; *Cormier*, 2007] and modeling of randomly oriented anisotropic patches [*Calvet and Margerin*, 2008]. A complexity in the observed travel-time data for polar PKP ray-paths [e.g. *Leykam et al*., 2010] leads to a conclusion that the IC may be a conglomerate of anisotropic domains [*Tkalčić*, 2010; *Mattesini et al*., 2013] as an alternative possibility to describe a significant variation in travel-times originating in the UIC.

6. Concluding remarks

In this study, we have used recordings from about 800 stations of the Hi-net

array stretching an elongated shape across the Japanese islands (over 15° degrees in latitude) originated from teleseismic earthquakes whose PKP_{DF} waves sample both “quasi-hemispheres” of the IC. This allowed us to construct individual complete empirical curves of PKP_{BC}-PKP_{DF} differential travel-times (BC-DF) for a total of 47 events whose waveforms passed our strict quality selection criteria. These empirical BC-DF curves show many elements of unprecedented observations in modern seismology as they consist of travel-times covering the theoretically predicted epicentral distance range, all from a single event. Through analysis of these travel-time curves, it becomes possible to critically examine and distinguish outer core and lowermost mantle effects from those that the IC structure imposes on travel-times of PKP_{DF} waves traversing its volume.

Our analysis reveals that both PREM and ak135 models could be adequate reference models for lowermost outer core velocity structure and that no significant modification of these models is necessary to explain the empirical BC-DF curves collected in this study. In addition, we have demonstrated that lowermost mantle structure is not responsible for variations in empirical BC-DF curves observed along the ray-paths analyzed in this study. Instead, a likely solution that emerges as most effective to match the observations is to modify

P-wave velocity in the UIC along each ray-path. Thus, our analysis leads to a conclusion that the IC could be heterogeneous laterally on global (hemispherical pattern), regional (few hundred kilometers) and possibly local scales (several tens of kilometers). The latter estimate is close to the estimate of heterogeneity size published in studies of PKiKP scattering in the upper part of the IC where heterogeneity scale lengths were found to be on the order of 1 to 10 km (e.g. *Leyton and Koper* [2007a]). We have quantified the minimum and maximum magnitude of lateral perturbations of P-wave velocity with respect to ak135 and PREM to be of 0.5-0.7% (0.8-0.9% with the lowermost mantle correction) in the QEH, and 1.4-1.7% (1.0-1.2% with the lowermost mantle correction) in the QWH.

The difference between the 1D models reported in this array-based study and the existing spherically symmetric Earth models (as well as the models for the QEH and the QWH) implies that the imaging of the IC has reached a stage similar to the imaging of the mantle, where simple homogeneous structures no longer provide adequate prediction of the growing seismological data. A further refinement of existing models is thus necessary to represent lateral and radial variations on both regional and local scales. Future installations of dense arrays such as the Hi-net array and corresponding array-studies will be a powerful tool

to image and clearly distinguish between anisotropy- and isotropic velocity heterogeneity-related effects on travel-times of core-sensitive body waves. This will then inevitably contribute to a better understanding of what the IC is made of and how it solidifies.

Chapter 3

Complex inner core of the Earth constrained by differential ray parameters

1. Introduction

Since the discovery of anomalous P-wave velocity in the Earth's inner core using differential traveltime of PKP(BC-DF) (Shearer et al., 1988), various studies using the same method have reported more complicated velocity structures of the inner core [e.g., Tanaka and Hamaguchi, 1997; Creager, 1997; Yu and Wen, 2007]. Beginning with the report that the P-wave velocity in the eastern hemisphere is faster than that in the western hemisphere [Tanaka and Hamaguchi, 1997],

However, these studies often do not agree with PKP(BC-DF, CD-DF) traveltime residuals depending on sampling areas and thus present different velocity structures of the inner core. For example, the traveltime residuals in regional and local scales showed different values even in the same hemispheres

with a consideration of the anisotropy. This naturally led to the speculation that the structure of the inner core would be very complicated regionally and locally, but we still have insufficient understanding about this argument.

The process of using differential traveltime has many advantages, which have contributed significant results so far. It is weakly sensitive to event source and not significantly affected by heterogeneous structure above the core-mantle boundary. However, it has obvious limitation in identifying sophisticated velocity structures. In general, the differential traveltime residual of globally sampled PKP(BC-DF, CD-DF) show scattering range more than 1 second. In consideration of this error boundary, it is difficult to distinguish the specific character into the velocity structure of the inner core. In order to overcome this problem, a recent study analyzed a well-constrained data from dense array with a narrow range of ray-angle and azimuth, showing the variation of the differential traveltime of PKP(BC-DF) on the scale of about hundred km and less [Yee et al., 2014]. This suggested about 1.5% Vp perturbation of uppermost 350 km of the inner core (UIC) in the same hemisphere, but it is still not enough to identify the precise and complicated velocity structure with considering the scattering range of about 0.5 second.

In addition, even if the scattering ranges are greatly reduced, there are myriad velocity structures that can fit a traveltime curve by changing velocities at various depths of the inner core. Another parameter that can constrain the velocity structure is needed to find a more accurate velocity structure of the inner core and the ray parameter (slowness) can be viable alternative. In ray theory the travel time curves are parameterized by the slowness and wave propagation in a horizontally stratified medium may be characterized by the slowness of the waves. The complete response of a stratified medium may also be represented as a superposition of cylindrical waves of varying slowness. This representation leads to the possibility of presenting the response of the stratification in a slowness time map containing both travel time and amplitude information. Such an approach requires copious good quality data but offers advantages in interpretation. Even in the presence of lateral variations of structure, slowness methods can provide useful information [Kennett, 1981].

Here we investigate the effect of velocity structures on traveltimes and ray parameters and find that the complex velocity structures of the inner core are constrained seldom by traveltimes. Because the ray parameters play important

role to identify the complex velocity structures, we perform Phase-Weighted Stack (PWS) the qualified waveforms and detect not only the differential traveltimes but also the differential ray parameters of PKP(BC-DF). These two parameters show significantly regional variations and we prove that such features are due to the velocity structure of the UIC, not due to other interference by using FK analysis. This indicates that the ray parameter curve can be an important parameter to identify the more accurate velocity structure of the inner core and our estimates of the heterogeneity spectrum represent invaluable new constraints on inner core structure.

2. Effect of velocity structure on traveltimes and ray parameters

In most previous studies, the velocity structures are inversed from the averaged traveltime curves that are sampled sparsely and easy to be biased due to the amount of data from specific regions. As a result, when the data was randomly resampled, the averaged traveltime curves showed very large uncertainties. Therefore, we investigate the effect of velocity structures on traveltimes and ray parameters first, which are perturbed ±1% in velocity at a total of 8 depth points, intervals of 50 km from the inner core boundary to 350 km depth. Some results from forward modeling based on ray tracing shows that even with very different

velocity structures produce similar traveltime curves but different features of ray parameter curves (Figure 3.1). This indicate that the ray parameter curves are very important parameter to constrain velocity structure and can play a very important role in obtaining more accurate velocity structures if used with traveltime curves.

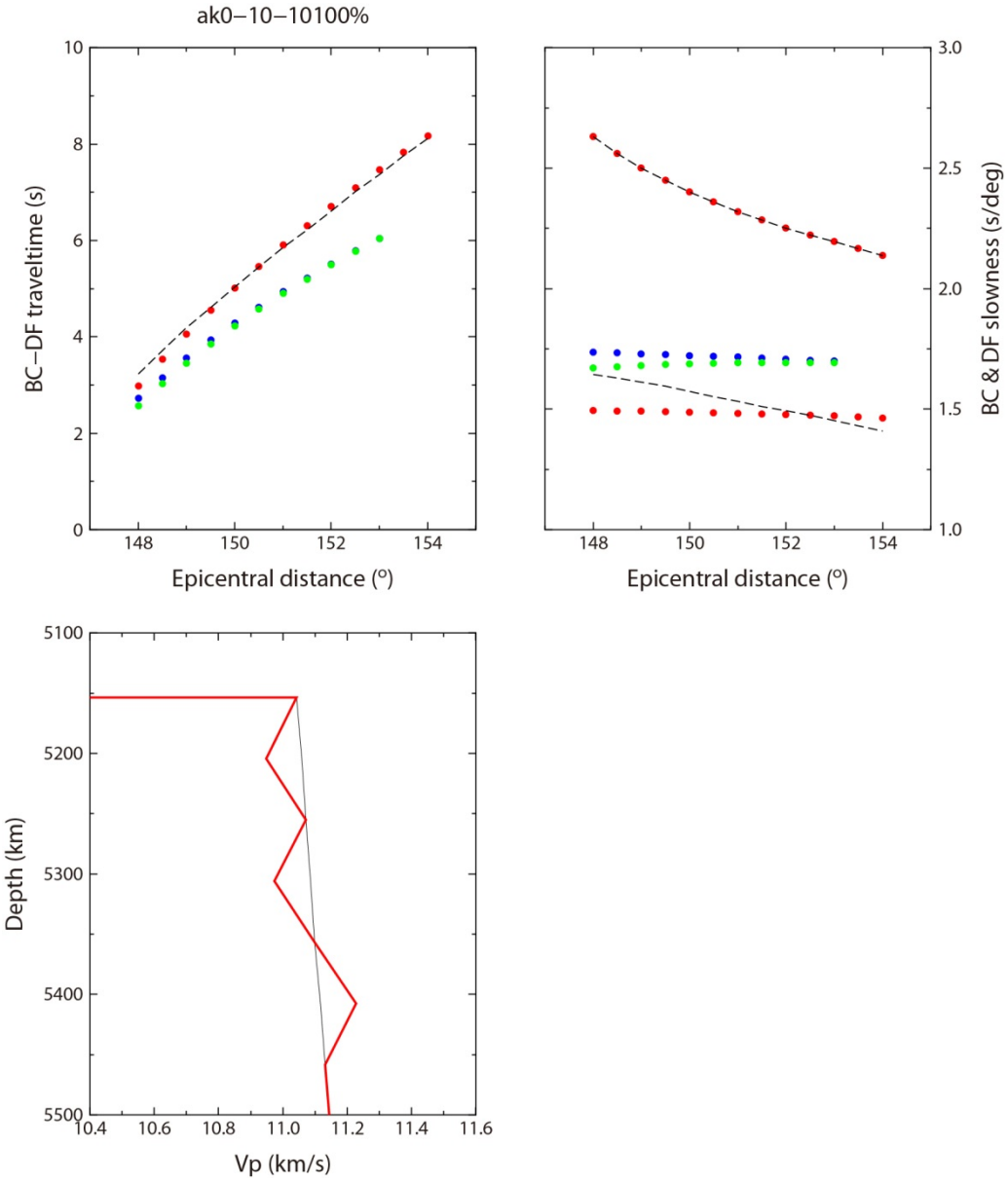

Figure 3.1. very different velocity structures produce similar traveltime curves but different features of ray parameter curves.

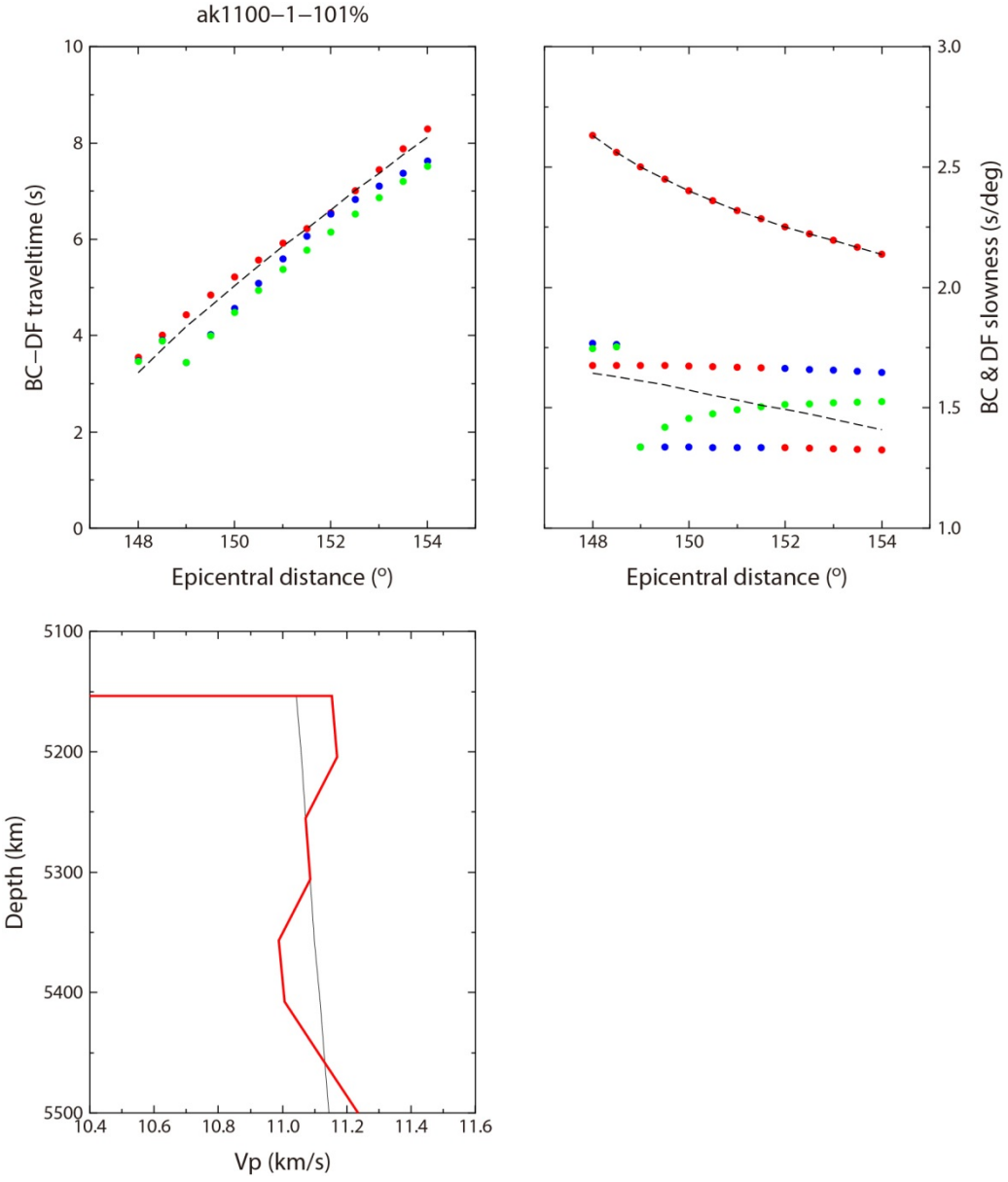

Figure 3.1. (continued)

3. Phase-Weighted Stack for Array data

To obtain both, the differential traveltimes and the differential ray parameters, we perform Phase-Weighted Stack (PWS) for same waveforms as Yee et al [2014] and try to confirm that the differential traveltimes obtained from the PWS method is same with previous ones from the cross correlation method. The configuration of Hi-net array and the location of large teleseismic earthquakes beneath southern Indian and northeastern Pacific Oceans deliver raypaths with near-equatorial sampling of the IC that span the epicentral distance range between 147° and 155° and sample both QEH and QWH of the inner core. The targeted events have the body wave magnitudes (mb) between 5.0 and 6.7. The waveforms from 47 individual events were selected with high criteria based on the correlation coefficient of BC and DF phases, signal-to-noise ratio (SNR), and visual inspection. Yee et al [2014] verified these waveforms through several investigations and showed significant traveltime variations in regional scale (~100 km) as a result of the systematic analysis.

The PWS is applied at pre-defined epicentral distances within a range of ±1.5°. The pre-defined epicentral distances are set from 148.0° to 154.0° with 0.5° interval (Figure 3.2). Because we measure the DF peaks by stacking, those are

regarded unbiased. We also perform bootstrap 500 times which resample same number of stations with replacement and measure means and standard deviations. The stacked range of ±1.5° is decided from tests for ±0.5°, ±1.0° and ±2.0°. In the range test, the standard deviation becomes smaller and stable as range increases. For ±0.5° and ±1.0°, the number of stacked waveforms is not enough and for ±2.0°, the measurements may average the possible important features which are shown in cases of smaller ranges. We measure 47 individual curves of the differential traveltime and ray parameter and assure those are well match with the previous result of the regional variations (Figure 3.3).

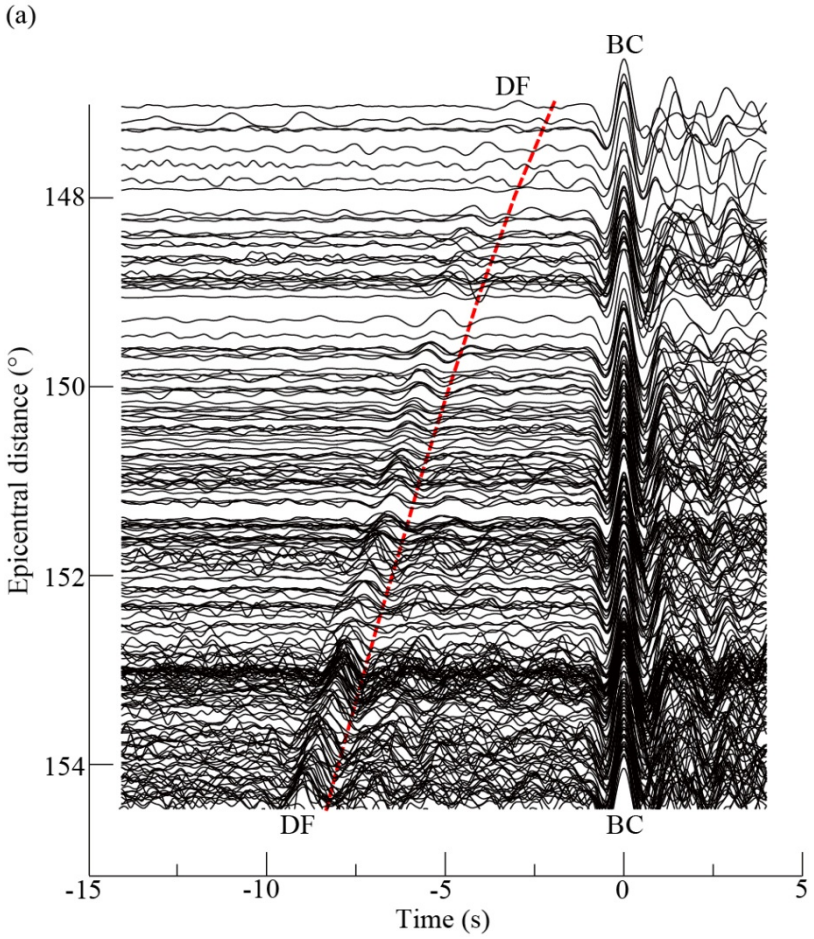

Figure 3.2. (a) All waveforms for an event are aligned with respect to the detected PKPBC phases. (b) phase-weighted stack at the pre-difined epicentral distances (c) residaul curves of differential traveltime and differential ray parameter from phase-weighted stack

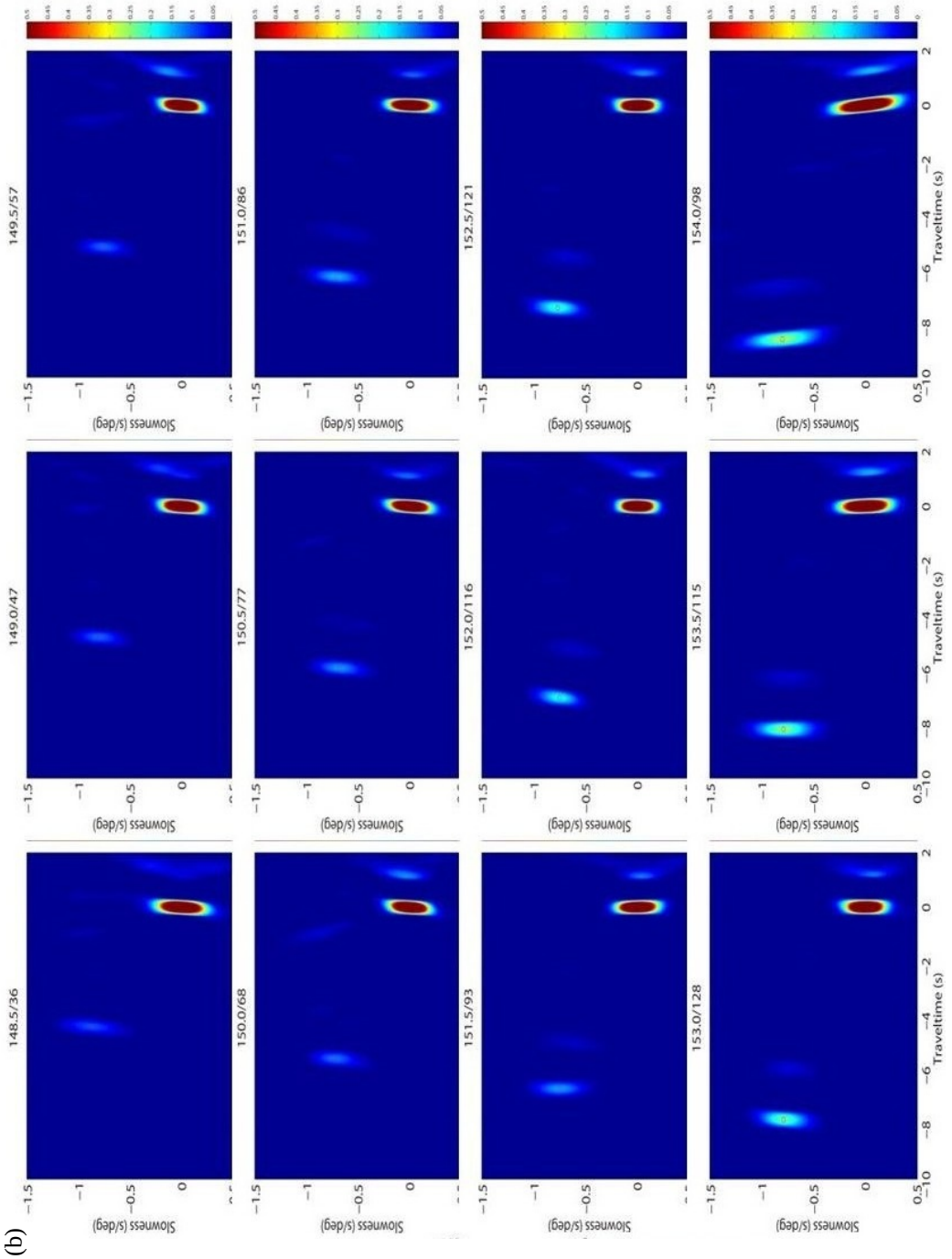

Figure 3.2. (continued)

(c)

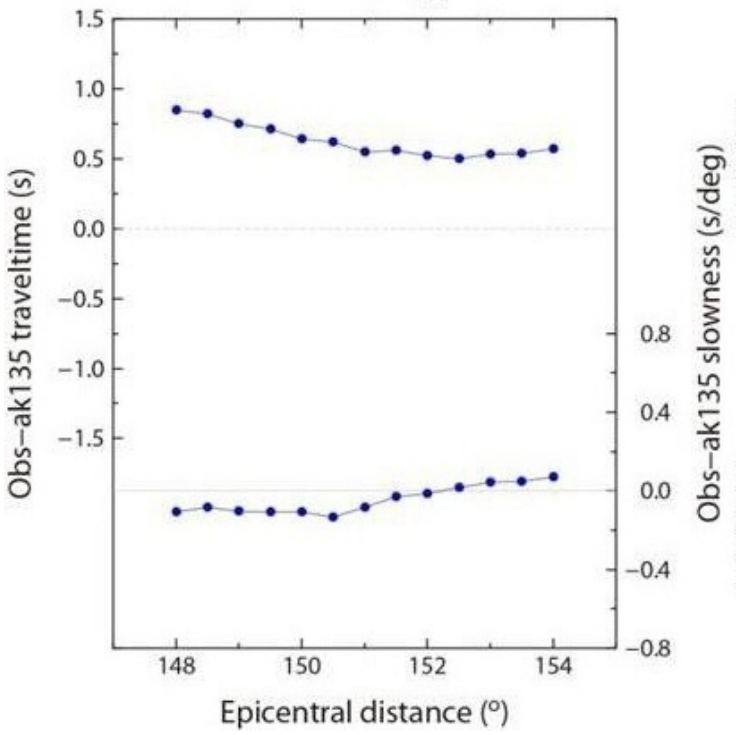

Figure 3.2. (continued)

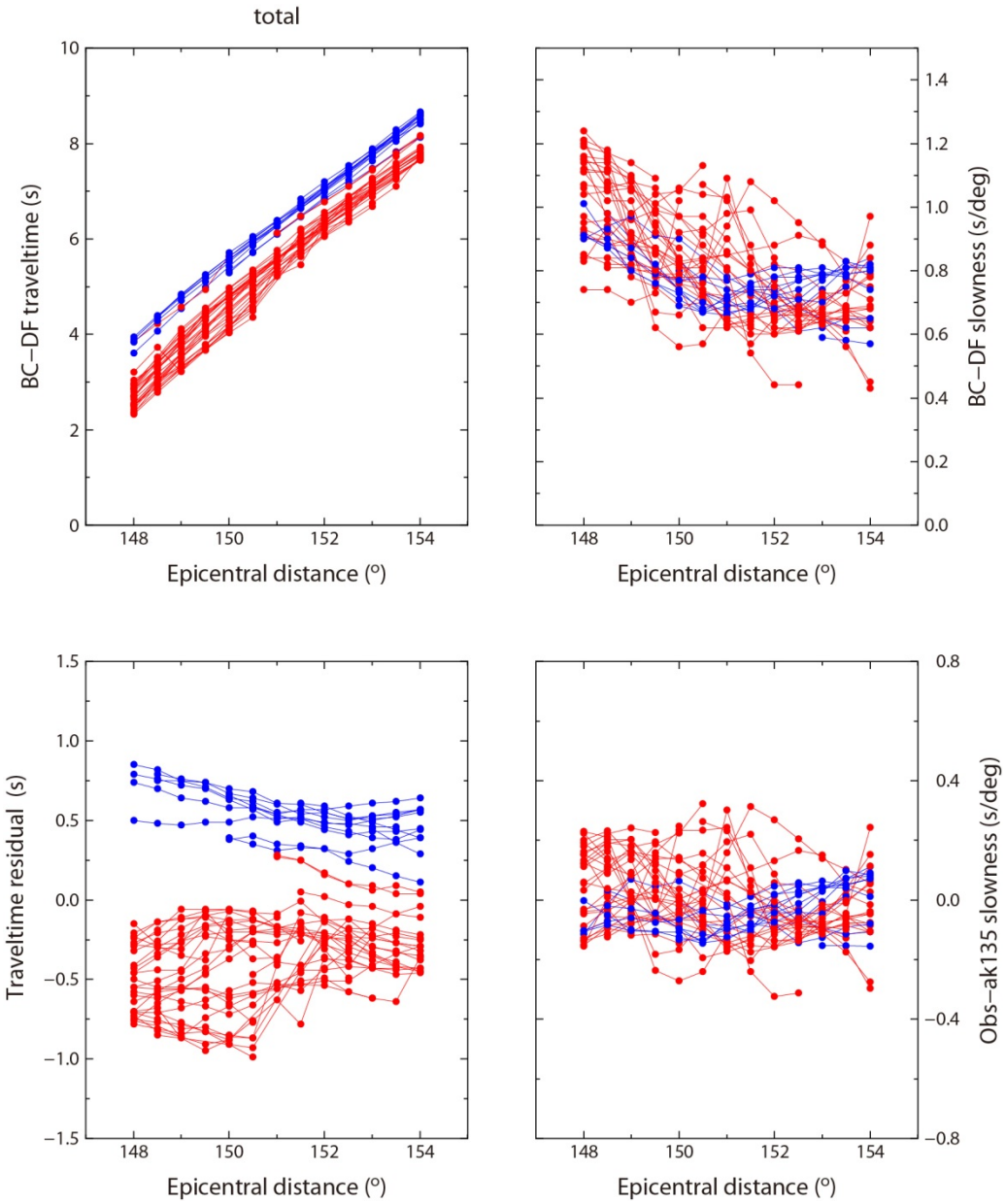

Figure 3.3. (top) 47 individual curves of the differential traveltime and ray parameter for the QEH (blue) and the QWH (red). (bottom) residuals of differential traveltimes and ray parameters. Those are well match with the previous result of the regional variations

4. Regional Variation of Ray parameter

Since the differential traveltimes obtained by the PWS is well matched with previous result, the differential ray parameters derived simultaneously from the same method are considered to be a reliable value. The ray parameter curves show a very large variation for each event. In order to quantitatively analyze this, we classify the ray parameter curves with correlation coefficient. Surprisingly, similar ray parameter curves showing high correlation locate very close, but it change significantly to different area (Figure 3.4). This supports the previous result that the traveltime residuals vary regionally and indicates that regional variations of the velocity structure exist in the inner core, which can change the BC-DF ray parameters.

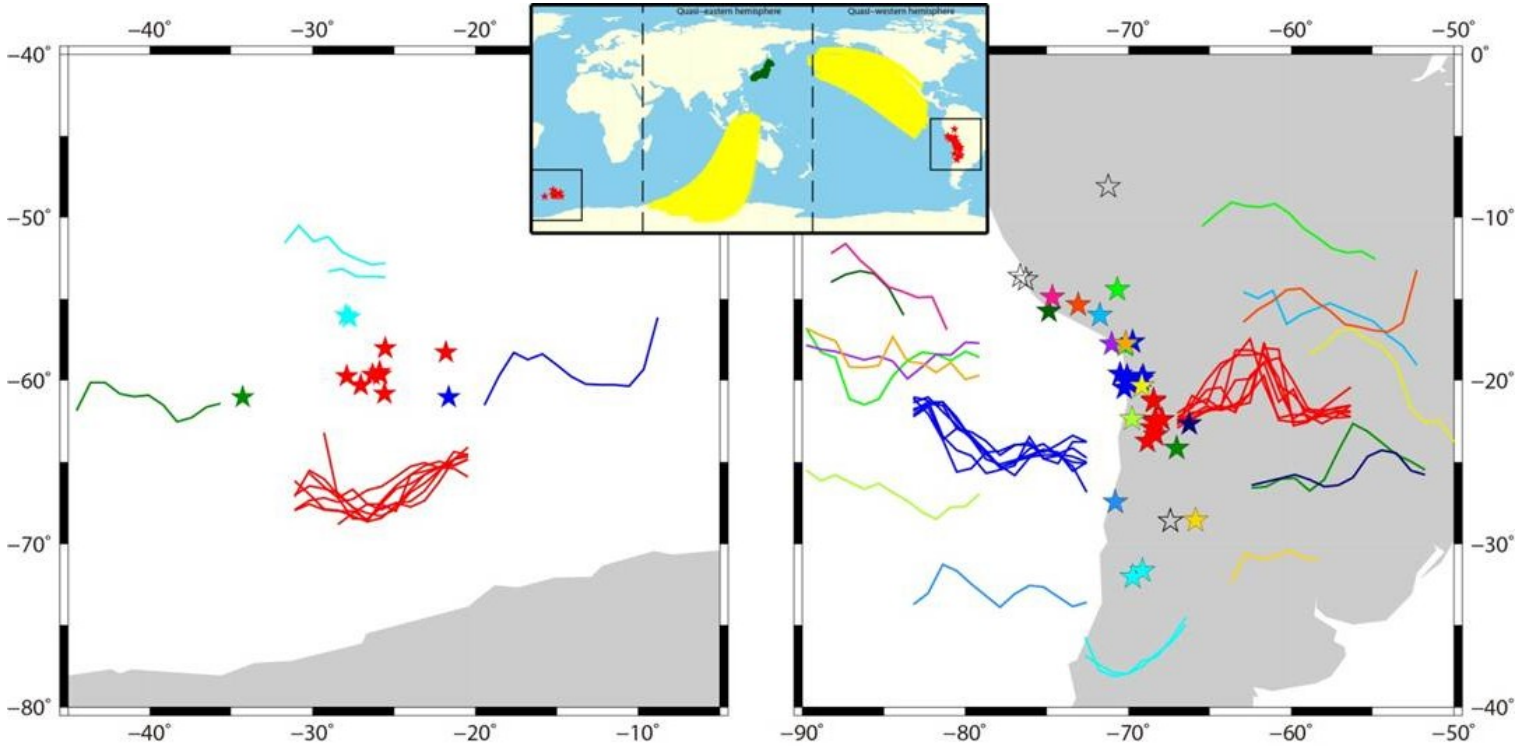

Figure 3.4. distribution of ray parameter curves for each event. similar ray parameter curves showing high correlation locate very close, but it change significantly to different area.

.4. Frequency-Wave number analysis

To confirm that the energy of the detected BC and DF is not due to other interference, FK analysis was applied using ±2 seconds waveforms from the BC and DF peak in the frequency range of 0.3 to 2.0 Hz. Back azimuths of the two phases are exactly matched (Figure 3.5). We also confirm that the back azimuths obtained from FK analysis for the total events show almost no difference with theoretical back azimuths from event-stations pair (Figure 3.6). In addition, the BC-DF ray parameters obtained from FK analysis is almost same as the ray parameters from PWS (Figure 3.7). This proves that the results from PWS are fairly reliable.

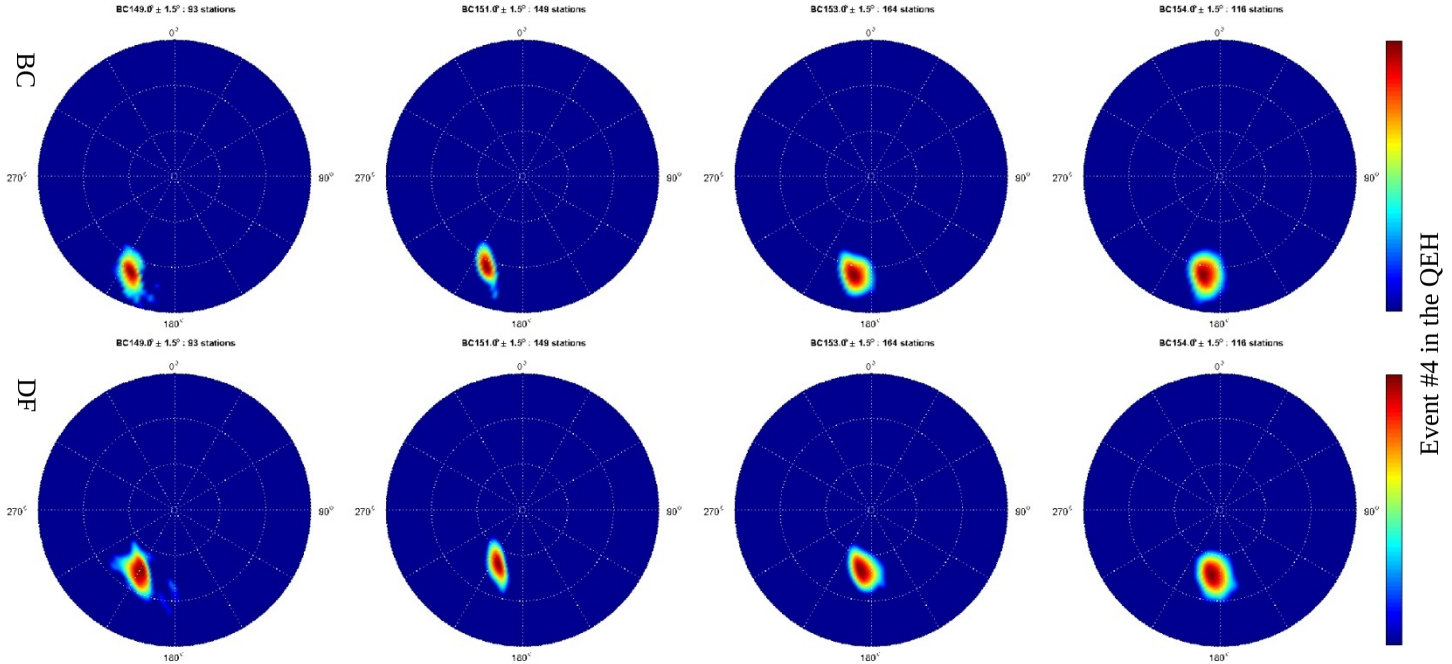

Figure 3.5. FK analysis was applied using ±2 seconds waveforms from the BC and DF peak for the QEH and the QWH.

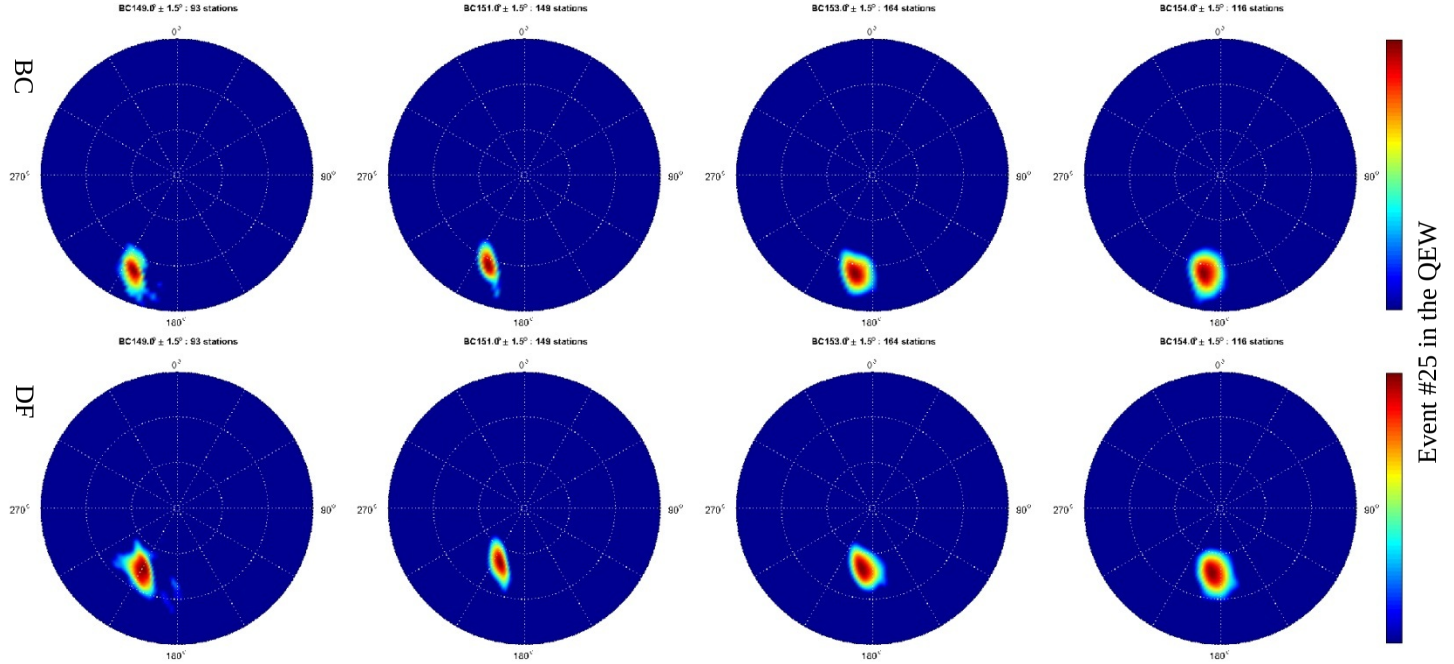

Figure 3.5. (continued)

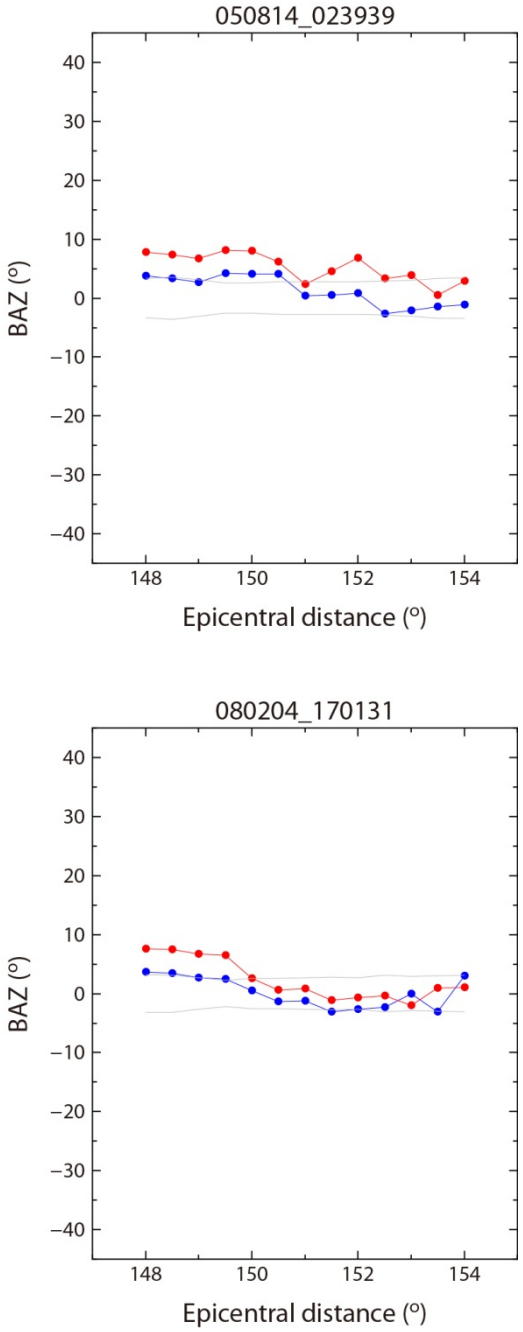

Figure 3.6. the back azimuths obtained from FK analysis for BC (blue) and DF (red). Grey line indicate standard deviations of theoretical back azimuths from event-stations pair.

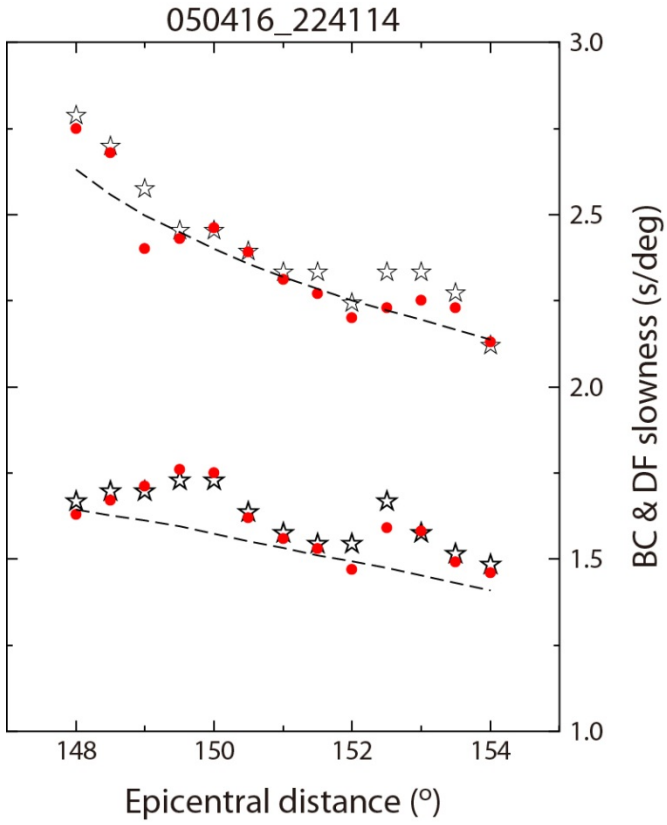

Figure 3.7. the BC-DF ray parameters obtained from FK analysis (star) is almost same as the ray parameters from PWS (red dot).

The interesting point is that the DF residuals are more perturbed than the BC residuals. The both residual curves show similar pattern, because the aforementioned advantages of the differential method have not been applied, calculating each phase separately may not remove the effects of the source, site or the structures of mantle and outer core properly. However, it is meaningful to show the intensely perturbed DF residuals in whole cases. In order to more precisely ensure this, the PWS was performed for BC and DF in absolute traveltime (Figure 3.8). If the residuals of traveltime and ray parameter are similar between the differential and absolute time, the measurements can be evaluated as reliable. Most of the results did not show any significant difference for the differential and absolute time, and we confirm that there was a larger deviation in the DF ray parameters. This proves that the local variation of the ray parameter is due to the structure of the UIC.

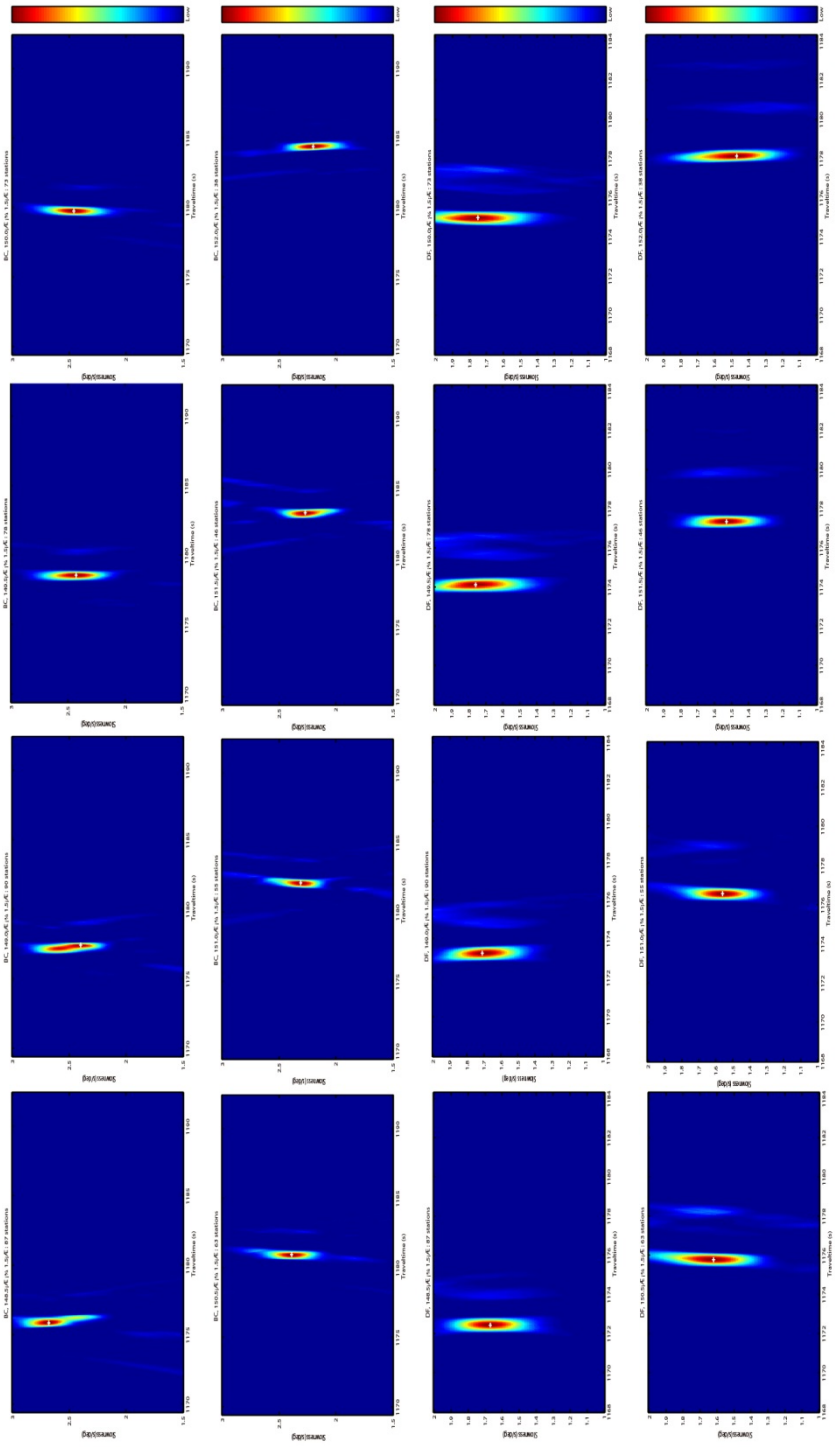

Figure 3.8. the PWS was performed for BC and DF in absolute traveltime.

5. Discussion & Conclusion

The regional variations of ray parameters are expected to contribute to further progressive result compared to the previous studies with only traveltime residuals which have estimated changed velocity structures at various depths in the inner core. Considering the fact that the distribution range of traveltime residuals is more than 1 second and the sampling areas are limited, these complicated velocity structures are hard to believe. Moreover, there are myriad velocity structures that can fit a traveltime curve by changing velocities at various points of the inner core, additional parameter that can constrain the velocity structure is needed to find a more complex velocity structure of the Earth's inner core and the ray parameter (slowness) can be viable alternative.

In this study, we have examined the effect of velocity structures on traveltimes and ray parameters, which are perturbed ±1% in velocity at a total of 8 depth points, intervals of 50 km from the inner core boundary to 350 km depth. The differential traveltimes is not enough to provide constraints for the complex velocity structures of the inner core and we suggest the ray parameters play important role to identify the complex velocity structures. We perform Phase-Weighted Stack the qualified waveforms and detect not only the differential

traveltimes but also the differential ray parameters of PKP(BC-DF). These two parameters show significantly regional variations and we prove that such features are due to the velocity structure of the UIC, not due to other interference by using FK analysis. This indicates that the ray parameter curve can be an important parameter to identify the more accurate velocity structure of the inner core and our estimates of the heterogeneity spectrum represent invaluable new constraints on inner core structure. The significant variations of the differential traveltimes and the differential ray parameters in the rate and level of solidification is a plausible physical outcome in an environment wherevigorous compositional convection in the outer core and variations in heat exchange across the inner core boundary may control the process of crystal growth. Further studies about possible heterogeneities that represent the regional variations from high-dimensional Vp structures are needed to explain these unique phenomena.

Chapter 4

Summary and Conclusion

In these thesis, I used recordings from about 800 stations of the Hi-net array stretching an elongated shape across the Japanese islands (over 15° degrees in latitude) originated from teleseismic earthquakes whose PKP_{DF} waves sample both “quasi-hemispheres” of the IC. This allowed me to construct individual complete empirical curves of PKP_{BC}-PKP_{DF} differential travel-times (BC-DF) for a total of 47 events whose waveforms passed our strict quality selection criteria. A forward modeling using grid search was performed to determine the P-wave velocity at the upper inner core (UIC) by reducing differential travel time residuals. The results show that P-wave velocities vary by 0.5 and 1.4% with respect to the earth reference models within the extent of about 660 and 910 km for the quasi-eastern and quasi-western hemispheres, respectively. These variations cannot be fully explained by possible errors including event locations, source time functions, mantle heterogeneities, and velocity structures in the outer core. In addition, the uniform cylindrical inner core anisotropy cannot explain our observations either and further studies will be necessary to understand the cause of existing heterogeneities in the UIC. In conclusion, this indicates that there are strong heterogeneities regionally or locally within the

Earth’s inner core.

However, observed differential travel times compiled from different studies showed wide deviations with respect to the mean values and this made it difficult to determine the heterogeneous structures in the inner core. In general, the differential traveltime residual of globally sampled PKP(BC-DF, CD-DF) show scattering range more than 1 second. In consideration of this error boundary, it is difficult to distinguish the specific character into the velocity structure of the inner core. In addition, previous study has a limitation that can only be expressed by averaged velocity profile in one dimension from the complex inner core structure. To constrain the complex structures of the inner core, we need more than one parameter. In ray theory, the ray parameter parameterize the travel time curves and wave propagation in a horizontally layered structure may be characterized by the ray parameter of the waves. This indicates that the ray parameter can be a key parameter. I apply the Phase-Weighted Stack to well-constrained waveforms and measure the differential traveltimes and the differential ray parameters in good agreement with previous study. I show that both, the differential traveltimes and the differential ray parameters, are influenced by high-dimensional heterogeneities of the inner core, not by the other structures. The existence of these variations of the

differential traveltimes and the differential ray parameters, which are highly sensitive in the region, indicates that the Earth's inner core is more complex than the conventional idea, and we need to approach with sophisticated modeling techniques in order to explain the nature of the inner core structure.

References

Alboussière, T., R. Deguen, and M. Melzani (2010), Melting induced stratification above the Earth's inner core due to convective translation, Nature, 466, 744–747.

Anderson, D. L., and R. S. Hart (1976), An Earth model based on free oscillations and body waves, J. Geophys. Res., 81, 1461–1475.

Aubert, J., H. Amit, G. Hulot, and P. Olson (2008), Thermochemical flows couple the Earth's inner core growth to mantle heterogeneity, Nature, 454, 758–761.

Bataille, K. and S. M. Flatte (1988), Inhomogeneities near the core–mantle boundary inferred from short-period scattered PKP waves recorded at the GDSN, J. Geophys. Res., 93, 15057–15064.

Bijwaard, H., W. Spakman, and E. R. Engdahl (1998), Closing the gap between regional and global travel-time tomography, J. Geophys. Res., 103, 30055–30078.

Bréger, L., B. Romanowicz, and H. Tkalčić (1999), PKP(BC-DF) travel time residuals and short scale heterogeneity in the deep Earth, Geophys. Res. Lett., 26, 3169–3172.

Bréger, L., H. Tkalčić, and B. Romanowicz (2000), The effect of D'' on PKP(AB–DF) travel-time residuals and possible implications for inner core structure, Earth Planet. Sci. Lett., 175, 133–143.

Calvet, M., Margerin, L. (2008), Constraints on grain size and stable iron phases in the uppermost inner core from multiple scattering modeling of seismic velocity and attenuation. Earth Planet. Sci. Lett., 267, 200–212.

Calvet, M., S. Chevrot, and A. Souriau (2006), P-wave propagation in transversely isotropic media II. Application to inner core anisotropy: Effects of data averaging, parameterization and a priori information, Phys. Earth Planet. Inter., 156, 21–40.

Cao, A., and B. Romanowicz (2004), Hemispherical transition of seismic attenuation at the top of the Earth's inner core, Earth Planet. Sci. Lett., 228, 243–253.

Cormier, V. F. (2007), Texture of the uppermost inner core from forward- and back-scattered seismic waves, Earth Planet. Sci. Lett., 258, 442– 453.

Cormier, V. F. and A. Stroujkova (2005), Waveform search for the innermost inner core, Earth Planet. Sci. Lett., 236, 96-105.

Cormier, V. F., and G. L. Choy, (1986), A search for lateral heterogeneity in the

inner core from differential travel-times near PKP-D and PKP-C, Geophys. Res. Lett., 13, 1553–1556.

Cormier, V. F., and X. Li (2002), Frequency-dependent seismic attenuation in the inner core: 2. A scattering and fabric interpretation, J. Geophys. Res., 107(B12), 2362.

Cormier, V. F., J. Attanayake and K. He (2011), Inner core freezing and melting: Constraints from seismic body waves, Phys. Earth Planet. Inter., 188, 163-172.

Creager, K. C. (1992), Anisotropy of the inner core from differential travel times of the phase PKP and PKIKP, Nature, 356, 309–314.

Creager, K. C. (1997), Inner core rotation rate from small-scale heterogeneity and time-varying travel-times, Science, 278, 1284–1288.

Creager, K. C. (1999), Large-scale variations in inner core anisotropy, J. Geophys. Res., 104, 23127–23139.

Deguen, R. (2012), Structure and dynamics of the Earth’s inner core, Earth Planet. Sci. Lett., 333–334, 211–225.

Deguen, R., T. Alboussière, and D. Brito (2007), On the existence and structure of a mush at the inner core boundary of the Earth, Phys. Earth Planet. Inter., 164, 36–49.

Deuss, A., J. C. E. Irving, and J. H. Woodhouse (2010), Regional variation of inner core anisotropy from seismic normal mode observations, Science, 328, 1018–1020.

Dziewonski, A., and D. L. Anderson (1981), Preliminary reference Earth model, Phys. Earth Planet. Inter., 25, 297–356.

Dziewonski, A., V. Lekic, and B. Romanowicz (2010), Mantle anchor structure: An argument for bottom up tectonics, Earth Planet. Sci. Lett., 299, 69–79.

Garcia, R. (2002), Constraints on upper inner core structure from waveform inversion of core phases. Geophys. J. Int., 150, 651–664.

Garcia, R., H. Tkalčić and S. Chevrot (2006), A new global PKP data set to study Earth's core and deep mantle, Phys. Earth Planet. Inter., 159, 15–31.

Garcia, R., S. Chevrot, and M. Calvet (2009), Statistical study of seismic heterogeneities at the base of the mantle from PKP differential traveltimes, Geophys. J. Int., 179, 1607–1616.

Garcia, R., Souriau, A. (2000), Inner core anisotropy and heterogeneity level, Geophys. Res. Lett., 27, 3121–3124.

Garnero, E.J. (2000), Heterogeneity of the lowermost mantle, Ann. Rev. Earth Planet Sci., 28, 509–537.

Haddon, R. A. W. and J. R. Cleary (1974), Evidence for scattering of seismic PKP waves near the mantle–core boundary, Phys. Earth Planet. Inter., 8, 211–234.

Helffrich, G., S. Kaneshima, and J.-M. Kendall (2002), A local, crossing-path study of attenuation and anisotropy of the inner core, Geophys. Res. Lett., 29(12), 1568.

Irving, J. C. E., and A. Deuss (2011), Hemispherical structure in inner core velocity anisotropy, J. Geophys. Res., 116, B04307.

Ishii, M. and A. M. Dziewonski (2002), The innermost inner core of the earth: evidence for a change in anisotropic behavior at a radius of about 300 km, Proc. Natl. Acad. Sci. U.S.A., 99, 14026–14030.

Ishii, M., A. M. Dziewonski (2005), Constraints on the outer-core tangent cylinder using normal-mode splitting measurements, Geophys. J. Int., 162, 787-792.

Ishii, M., A. M. Dziewonski, J. Tromp, and G. Ekstrom (2002), Joint inversion of normal mode and body wave data for inner core anisotropy, 2, Possible complexities, J. Geophys. Res., 107, 2380.

Isse, T., I. Nakanishi (2002), Inner-core anisotropy beneath Australia and

differential rotation, Geophys. J. Int., 151, 255–263.

Jeanloz, R., H.-R. Wenk (1988), Convection and anisotropy of the inner core, Geophys. Res. Lett., 15, 72–75.

Jeffreys, H. (1939), The times of the core waves (second paper), Mon. Not. R. Astron. Soc., Geophys. Suppl., 4, 594– 615.

Kaneshima, S. (1996), Mapping heterogeneity of the uppermost inner core using two pairs of core phases, Geophys. Res. Lett., 23, 3075–3078.

Kárason, H., and R. D. van der Hilst (2001), Tomographic imaging of the lowermost mantle with differential times of refracted and diffracted core phases (PKP, Pdiff), J. Geophys. Res., 106, 6569–6587.

Kawakatsu, H. (2006), Sharp and seismically transparent inner core boundary region revealed by an entire network observation of near-vertical PKiKP, Earth Planets Space, 58, 855–863.

Kazama, T., H. Kawakatsu, and N. Takeuchi (2008), Depth-dependent attenuation structure of the inner core inferred from short-period Hi-net data, Phys. Earth Planet. Inter., 167, 155–160.

Kennett, B. L. N. (1981), Slowness techniques in seismic interpretation, J. Geophys. Res., 86(B12), 11575–11584.

Kennett, B. L. N. and E. R. Engdahl (1991), Traveltimes for global earthquake location and phase identification, Geophys. J. Int., 105, 429–465.

Kennett, B. L. N., E. R. Engdahl, and R. Buland (1995), Constraints on seismic velocities in the Earth from traveltimes, Geophys. J. Int., 122, 108–124.

Krasnoshchekov, D. N., P. B. Kaazik and V. M. Ovtchinnikov (2005), Seismological evidence for mosaic structure of the surface of the Earth's inner core, Nature, 435, 483-487.

Lay, T., Q. Williams, and E. J. Garnero (1998), The core-mantle boundary layer and deep Earth dynamics, Nature, 392, 461–468.

Lehmann, I., (1936), P', Bur. Cent. Seismol. Int. A, 14, 87–115.

Leykam, D., H. Tkalčić and A.M. Reading (2010), Core structure reexamined using new teleseismic data recorded in Antarctica: Evidence for, at most, weak cylindrical seismic anisotropy in the inner core, Geophys. J. Int., 180, 1329-1343.

Leyton, F., and K. D. Koper (2007a), Using PKiKP coda to determine inner core structure: 1. Synthesis of coda envelopes using single-scattering theories, J. Geophys. Res., 112, B05316.

Leyton, F., and K. D. Koper (2007b), Using PKiKP coda to determine inner

core structure: 2. Determination of QC, J. Geophys. Res., 112, B05317.

Li, C., R. D. van der Hilst, E. R. Engdahl, and S. Burdick (2008), A new global model for P wave speed variations in Earth's mantle, Geochem. Geophys. Geosyst., 9, Q05018.

Mattesini, M., A. B. Belonoshko, H. Tkalčić, E. Buforn, A. Udías, and R. Ahuja (2013), Candy wrapper for the Earth's inner core, Sci. Rep., 3, 2096.

Monnereau, M., M. Calvet, L. Margerin, and A. Souriau (2010), Lopsided growth of Earth's inner core, Science, 328, 1014–1017.

Morelli, A., A. M. Dziewonski, and J. H. Woodhouse (1986), Anisotropy of the inner core inferred from PKIKP travel-times, Geophys. Res. Lett., 13, 1545–1548.

Müller, G. (1973), Amplitude studies of core phases, J. Geophys. Res., 78, 3469–3490.

Niu, F., and L. Wen (2001), Hemispherical variations in seismic velocity at the top of the Earth's inner core, Nature, 410, 1081–1084.

Niu, F., and L. Wen (2002), Seismic anisotropy in the top 400 km of the inner core beneath the ‘‘eastern’’ hemisphere, Geophys. Res. Lett., 29, 1611.

Obayashi, M., and Y. Fukao (1997), P and PcP travel-time tomography for the

core-mantle boundary, J. Geophys. Res., 102, 17825–17841.

Ohtaki, T., S. Kaneshima, and K. Kanjo (2012), Seismic structure near the inner core boundary in the south polar region, J. Geophys. Res., 117, B03312.

Okada, Y, K. Kasahara, S. Hori, K. Obara, S. Sekiguchi, H. Fujiwara, and A. Yamamoto (2004), Recent progress of seismic observation networks in Japan - Hi-net, F-net, K-NET and KiK-net -, Earth, Planets and Space, 56, xv-xviii.

Oreshin, S. I., and L. P. Vinnik (2004), Heterogeneity and anisotropy of seismic attenuation in the inner core, Geophys. Res. Lett., 31, L02613.

Peng, Z., K. D. Koper, J. E. Vidale, F. Leyton, and P. Shearer (2008), Inner-core fine-scale structure from scattered waves recorded by LASA, J. Geophys. Res., 113, B09312.

Poupinet, G., R. Pillet, and A. Souriau (1983), Possible heterogeneity of the Earth's core deduced from PKIKP travel-times, Nature, 305, 204–206.

Qamar, A. (1973), Revised velocities in the Earth's core, Bull. Seism. Soc. Am., 63, 1073–1105.

Romanowicz B., H. Tkalčić and L. Breger (2003), On the origin of complexity in PKP travel-time data from broadband records, AGU volume on inner core and lower mantle, AGU Geodynamics Series, V. Dehant, K. Creager, S. Karato,

S. Zatman, Editors.

Romanowicz, B., X.-D. Li, J. Durek (1996), Anisotropy in the inner core: Could it be due to low-order convection?, Science, 274, 964–966.

Rost, S., and C. Thomas (2002), Array seismology: Methods and application, Rev. Geophys., 40, 1008.

Shearer, P. M., and K. M. Toy, (1991), PKP(BC) versus PKP(DF) differential travel-times and aspherical structure in the Earth's inner core, J. Geophys. Res., 96, 2233–2247.

Soldati, G., L. Boschi, and A. M. Forte (2012), Tomography of core–mantle boundary and lowermost mantle coupled by geodynamics. Geophys. J. Int., 189, 730–746.

Song, X. D., and D. V. Helmberger (1998), Seismic evidence for an inner core transition zone, Science, 282, 924–927.

Souriau, A. (2007), Treatise on Geophysics, 1, Ch. The Earth’s Core, Elsevier, 655–693.

Souriau, A. and G. Poupinet (1991), The velocity profile at the base of the liquid core from PKP(BC+Cdiff) data: an argument in favor of radial inhomogeneity. Geophys. Res. Lett., 18, 2023–2026.

Souriau, A., A. Teste, and S. Chevrot (2003) Is there any structure inside the liquid core? Geophys. Res. Lett., 30(11), 1567.

Stevenson, D. (1987), Limits on lateral density and velocity variations. Geophys. J. R. Astr. Soc. 88, 311–319.

Stroujkova A. and V. F. Cormier (2004), Regional variations in the uppermost 100 km of the Earth’s inner core, J. Geophys. Res., 109, B10307.

Su, W. J., A. M. Dziewonski (1997), Simultaneous inversion of 3-D variations in shear and bulk velocity in the mantle, Phys. Earth Planet. Inter., 100, 135–156.

Tanaka, S. (2004), Seismic detectability of anomalous structure at the top of the Earth's outer core with broadband array analysis of SmKS phases. Phys. Earth Planet. Inter. 141, 141–152.

Tanaka, S. (2007), Possibility of a low P-wave velocity layer in the outermost core from global SmKS waveforms, Earth Planet. Sci. Lett., 259, 486–499.

Tanaka, S., and H. Hamaguchi (1997), Degree one heterogeneity and hemispherical variation of anisotropy in the inner core from PKP (BC)-PKP (DF) times, J. Geophys. Res., 102, 2925–2938.

Tkalčić, H. (2010), Large variations in travel-times of mantle-sensitive seismic

waves from the South Sandwich Islands: Is the Earth's inner core a conglomerate of anisotropic domains?, Geophys. Res. Lett., 37, L14312.

Tkalčić, H. and B. L. N. Kennett (2008), Core structure and heterogeneity: seismological perspective, Austral. J. Earth Sci., 55:4, 419-431.

Tkalčić, H., Romanowicz, B. and Houy, N. (2002), Constraints on D'' structure using PKP(AB–DF), PKP(BC–DF) and PcP–P travel-time data from broad-band records, Geophys. J. Int., 149, 599–616.

Tromp, J. (1993), Support for anisotropy of the Earth's inner core from free oscillations, Nature, 366, 678–681.

Vidale, J. E., and P. S. Earle (2000), Fine-scale heterogeneity in the Earth's inner core, Nature, 404, 273–275.

Waszek, L., and A. Deuss (2011), Distinct layering in the hemispherical seismic velocity structure of Earth's upper inner core, J. Geophys. Res., 116, B12313.

Woodhouse, J. H., D. Giardini, and X.-D. Li (1986), Evidence for inner core anisotropy from free oscillations, Geophys. Res. Lett., 13, 1549–1552.

Wookey, J., and G. Helffrich (2008), Inner-core shear-wave anisotropy and texture from an observation of PKJKP waves, Nature, 454, 873–876.

Wysession, M. E. (1996), Large-scale structure at the core–mantle boundary

from diffracted waves, Nature, 382, 244–248.

Yee, T.-G., J. Rhie, and H. Tkalčić (2014), Regionally heterogeneous uppermost inner core observed with Hi-net array, J. Geophys. Res. Solid Earth, 7823–7845, 119,

Yoshida, S., I. Sumita, M. Kumazawa (1996), Growth model of the inner core coupled with outer core dynamics and the resulting elastic anisotropy, J. Geophys. Res., 101, 28085–28103.

Young, M. K., H. Tkalčić, T. Bodin, and M. Sambridge (2013), Global P wave tomography of Earth's lowermost mantle from partition modeling, J. Geophys. Res., 118, 5467–5486,

Yu, W., and L. Wen (2006), Seismic velocity and attenuation structures in the top 400 km of the Earth's inner core along equatorial paths, J. Geophys. Res., 111, B07308.

Yu, W., L. Wen, and F. Niu (2005), Seismic velocity structure in the Earth's outer core, J. Geophys. Res., 110, B02302.

Zou, Z., K. D. Koper, and V. F. Cormier (2008), The structure of the base of the outer core inferred from seismic waveforms diffracted around the inner core, J. Geophys. Res., 113, B05314.

국문초록

지구 내핵의 속도 구조와 그 체적 변이에 대한 연구는 내핵의 동역학과 조성에 대한 우리의 이해를 조명한다. 이 논문에서 우리는 완전한 PKPbc-PKPdf 주시 차 곡선을 구성하기 위해 일본의 하이넷 어레이에 기록된 광범위한 지진 기록을 이용하였다. 이 주시 차 곡선은 PKPdf 파가 내핵의 상부를 통과하는 동안 중요한 변이들이 주시에 누적되는 반면 외핵의 구조에 의한 영향은 상대적으로 덜 받는다는 특징을 지니고 있다. 샘플링된 파선 각도의 범위가 굉장히 제한적이기 때문에, 관측된 주시 차의 변이는 내핵에 존재하는 원통형 이방성의 영향을 받은 것이 아니라 해석할 수 있다. 최신 토모그래픽 모델을 통해 알려진 맨틀 최하부 비균질성의 구성과 강도 역시 관측된 주시 차의 변이를 설명 하기엔 한계가 있다. 따라서, 우리는 상부 내핵 약 100km 이내의 공간 안에 P파 등방성 속도의 변이가 존재하거나 혹은 그 구성 물질이 특유의 이방성 조각들로 구성되어 있을 수 있으며, 이러한 구조적 특징들이 반구에 달하는 길이에 걸쳐 중첩되어 존재할 수 있

다고 생각한다. 만약 속도의 변이만 존재한다고 가정한다면 P파의 속도 변이의 정도는 준-동반구에서 0.60±0.10 %, 준-서반구에서 1.55±0.15 % (최하부 맨틀 보정을 했을 경우 각각 0.85±0.05 %, 1.10 ± 0.10 %)로 계산되었으며 이러한 변이의 존재는 외핵에서의 활발한 조성 대류와 그에 따른 내핵 경계에서의 열교환 변이가 결정화 과정을 제어하는 주 요인임을 생각한다면 물리적으로 상당히 합리적인 결과라고 할 수 있다. 이 결과를 통해 지역적으로 존재하는 비균질성의 존재를 보여 주는데는 성공하였으나, 이러한 비균질체의 정확한 위치와 크기는 주시 차의 변이만을 사용해서는 규명하기 어렵다. 이 한계를 극복하기 위해, PKPbc-PKPdf 주시 차 뿐만 아니라 파선 변수 차를 사용하여 내핵 최상부의 P파 속도 구조를 연구하였다. 하이넷 어레이에 기록된 파형에 대하여 위상 가중 중첩법을 수행하여 파선 변수 차를 측정하였으며 그 값 역시 두 반구 내에서 지역적 변이를 보이고 있었다. 이 관측 결과는 주시 차만을 이용한 이전 결과와도 잘 들어맞을 뿐 아니라 복잡한 P파 속도 구조에 대한 추가 제한 조건을 제공한다. 우리는 관측된 주시 차와 파선 변수 차의 지역적 변이를 모사하기 위해 내핵 경계 지형과 곤죽 지대를 포함하여 다양한 비균질체

를 가진 다수의 2-D 모델을 조사하였다. 내핵의 비균질성에 대한 폭넓은 우리의 추정은 내핵 구조에 대한 새로운 열쇠를 제시한다는 점에서 매우 중요한 의의가 있다.

주요어: 지구 내핵, PKPdf, PKPbc, 주시 차, 파선 변수 차, P파 속도 변이, 등방적 비균질성, 위상 가중 중첩법

학 번: 2010-30110